

**NATURAL, FORCED AND MIXED CONVECTION IN A VERTICAL
CROSS-CORRUGATED CHANNEL**

By

Yinghu Piao

B. Sc. (Thermal Energy Engineering) Tianjin University, China

M. Sc. (Thermal Energy Engineering) Tianjin University, China

**A THESIS SUBMITTED IN PARTIAL FULFILLMENT OF
THE REQUIREMENTS FOR THE DEGREE OF
MASTER OF APPLIED SCIENCE**

in

**THE FACULTY OF GRADUATE STUDIES
MECHANICAL ENGINEERING**

We accept this thesis as conforming
to the required standard

THE UNIVERSITY OF BRITISH COLUMBIA

August 1992

© Yinghu Piao, 1992

In presenting this thesis in partial fulfilment of the requirements for an advanced degree at the University of British Columbia, I agree that the Library shall make it freely available for reference and study. I further agree that permission for extensive copying of this thesis for scholarly purposes may be granted by the head of my department or by his or her representatives. It is understood that copying or publication of this thesis for financial gain shall not be allowed without my written permission.

Mechanical Engineering
The University of British Columbia
2075 Wesbrook Place
Vancouver, Canada
V6T 1W5

Date:

Sept. 10, 1992

ABSTRACT

Natural, forced and mixed convection heat transfer in a vertical cross-corrugated channel have been experimentally studied, using air as a working fluid. The channel is formed by two transversely positioned corrugated sheets and two flat side-walls which are thermally insulated. The thermal boundary condition is asymmetric and is such that one sheet is radiant-heated and the other is thermally insulated. A hot-wire anemometer and thermocouples were used to measure the fluid velocity and temperature, as well as the wall temperature. The local heat flux across the heated corrugated sheet was also measured with heat flow sensors.

In the natural convection experiments, the effect of channel gap on heat transfer was studied. The results show that the Nusselt number Nu_L based on channel length was larger at the smaller gap than at the larger gap under natural convective flow. This may be due to the specific geometry of the cross-corrugated channel; the boundary layer of the fluid develops from the heated sheet and interacts with the other insulated sheet. For the smaller gap, the interaction of the boundary layer is probably more vigorous compared to the case of the larger gap, which eventually changes the flow pattern and increases the heat transfer.

Under forced convection, a heat transfer correlation has been developed and a comparison was made with other similar work. A high heat transfer coefficient in this cross-corrugated channel was achieved with a reasonable value of the friction factor. Local

heat transfer rate on the heated corrugated sheet was measured at several different locations with heat flow sensors. The result showed that local heat flux at the valley of the corrugation was less than that at the peak. The ratio of these two heat fluxes was correlated with Reynolds number, and the difference of these two heat fluxes became small as Reynolds number increases in the present experimental range.

Mixed convection has been presented in a way which allows comparison to the 'pure' forced convection. Mixed convection in the cross-corrugated channel has shown similar phenomena as buoyancy-aided pipe flow. Natural convection effect on mixed convection was very small in this experimental range.

Table of Contents

ABSTRACT	ii
List of Tables	vii
List of Figures	viii
Acknowledgement	x
NOMENCLATURE	xi
1 INTRODUCTION	1
2 LITERATURE SURVEY	3
2.1 Natural convection	3
2.2 Forced convection	8
2.3 Mixed convection	11
2.4 Scope of the present study	13
3 EXPERIMENTAL APPARATUS	14
3.1 Experimental apparatus	14
3.1.1 Corrugated sheets	14
3.1.2 Working fluid	16
3.2 Test section and heating equipment	16
3.2.1 Extension channel	18
3.2.2 Fan assembly	20

3.3	Measurements	20
3.3.1	Wall temperature measurement	20
3.3.2	Wall heat flux measurement	20
3.3.3	Pressure drop measurement	21
3.3.4	Air velocity and temperature measurements	22
3.3.5	Data acquisition system	25
3.4	Calibration of instruments	25
3.5	Experimental procedure	30
4	EXPERIMENTAL RESULTS AND DISCUSSIONS	32
4.1	Calculations in the heat transfer correlations	32
4.1.1	Mean velocity at the inlet of the channel U_0	32
4.1.2	Bulk temperature of air at the outlet of the channel T_{bo}	33
4.1.3	Heat transfer rate Q	34
4.2	Results and discussions	34
4.2.1	Natural convection	35
4.2.2	Forced convection	39
4.2.3	Mixed convection	44
4.2.4	Pressure drop and friction factor	48
4.2.5	Local heat transfer rate on the heated wall	51
5	CONCLUSIONS	55
5.1	Natural convection	55
5.2	Forced convection	56
5.3	Mixed convection	57
6	RECOMMENDATIONS	58

6.1	Experimental apparatus	58
6.2	Future work	59
	Bibliography	61
	Appendices	64
	A Sample Calculation	64
A.1	Wall temperature	66
A.2	Mean velocities and bulk temperatures of the fluid	68
A.3	Sample calculation	70
	B Error analysis	72
B.1	Wall temperature measurement	72
B.2	Air velocity measurement	73
B.3	Bulk air temperature measurement	75
B.4	Heat transfer rate	77
B.5	Dimensionless terms	77
	C Estimation of Radiation Heat Transfer	81
	D Estimation of Heat Loss through the Insulated Walls	84
D.1	Heat loss through the extension channel	84
D.2	Heat loss through the cross-corrugated channel	87

List of Tables

2.1	Three characteristic natural convective flow situations.	6
2.2	Some typical channel geometries and correlations.	10
3.3	Output of heat flow sensors at surface temperature of 20°C.	27
3.4	Specifications of hot wire/film probes.	28
3.5	Calibration conditions of the probes.	29
3.6	Constants in Eq.(3.15).	30
4.7	Specifications of channel gaps.	35
4.8	Comparison of Nusselt number Nu	44
A.9	The original data from data acquisition.	65
B.10	Summary of error analysis.	80

List of Figures

3.1	Schematic diagram of the experimental apparatus.	15
3.2	Profile of the corrugated sheet.	16
3.3	Schematic diagram of the test section.	17
3.4	The channel hydraulic gap b and the minimum gap b_{min}	19
3.5	Position of thermocouple wires and heat flow sensors.	21
3.6	Position of pressure taps.	22
3.7	Position of hot-wire and thermocouple wire probes.	23
3.8	Schematic of data acquisition system.	26
3.9	Output multiplication factor vs. surface temperature.	27
3.10	Calibration curves for hot wire/film probes.	29
4.11	Relation between Nu_b and Ra_b in natural convection.	37
4.12	Relation between Nu_L and Ra_L in natural convection.	38
4.13	Heat transfer correlation for forced convection.	41
4.14	Relation between Nu_D and Re_D in forced convection.	42
4.15	Heat transfer relation for mixed convection.	47
4.16	Axial pressure distribution in the corrugated channel.	49
4.17	Relation between friction factor ξ and Re_D	50
4.18	Local heat flow rate along the flow direction.	52
4.19	Local heat flux ratio variation with Re_D for gap2.	54
A.20	Wall temperature distribution on the heated sheet.	66
A.21	Air velocity and temperature profiles.	69

D.22 Heat loss through the extension channel. 85

Acknowledgement

I wish to thank Dr. M. Iqbal and Dr. E. G. Hauptmann for their supervision through all stage of this work.

My sincere thank also goes to Mr. K. Zhang for his generous help in the computer data acquisition programming and my friends and families for their various kinds of support.

Financial support for this work by the Natural Sciences and Engineering Research Council of Canada is gratefully acknowledged.

NOMENCLATURE

L	length of the corrugated channel (m)
W	width of the corrugated channel (m)
b	gap of the corrugated sheets (m)
D_h	hydraulic diameter of the corrugated channel (m)
b_e	spacing of the extension channel (m)
q	heat flux (W/m^2)
Q	heat flow rate (W)
u	local air velocity (m/s)
U	mean velocity of the air (m/s)
T	temperature (°C, K)
ΔT	temperature difference (°C, K)
E	bridge voltage of a hot-wire anemometer (V)
R	resistance of the bridge (Ω)
l	length of sensing area of hot wire/film (mm)
d	diameter of hot wire/film (μm)
P	pressure (N/m^2)
p	pressure (bar or atm)
g	gravitational acceleration (m/s^2)
h	vertical height of alcohol column (m)
B, C, n, m	constants
A	area (m^2)
x, y, z	Cartesian coordinates

S	standard deviation
ε	error
γ	temperature coefficient of a hot wire/film (1/K)
ρ	density of the fluid (kg/m ³)
c_p	specific heat of the fluid (J/kg °C)
k	thermal conductivity of the fluid (W/m °C)
β	coefficient of thermal expansion (1/K)
ν	kinematic viscosity (m ² /s)
α	thermal diffusivity of the fluid (m ² /s)
ϵ	emittance
σ	Stefan-Boltzmann constant (= 5.67×10^{-8} W/m ² K ⁴)
ϕ	relative humidity of the atmosphere
Re	Reynolds number
Gr	Grashof number
Pr	Prandtl number
Ra	Rayleigh number
Nu	Nusselt number

Subscripts

D	(hydraulic) diameter
L	length of the corrugated channel
e	extension channel

<i>w</i>	heated corrugated wall
∞	ambient condition
<i>i</i>	inlet of the channel
<i>o</i>	outlet of the channel
<i>b</i>	bulk (temperature), gap (of a channel)
<i>f</i>	fluid
<i>F</i>	forced
<i>film</i>	film (temperature)
<i>0</i>	inlet condition
<i>cal</i>	calibration
<i>wire</i>	hot wire/film
<i>c</i>	correction
<i>min</i>	minimum
<i>max</i>	maximum
<i>m</i>	mean
<i>mb</i>	mean beam
<i>wv</i>	water vapor
<i>s</i>	saturation
<i>l</i>	loss
<i>r</i>	radiation
<i>Al</i>	alcohol
<i>T</i>	temperature
<i>Q</i>	heat flow rate
<i>u</i>	local air velocity
<i>U</i>	mean velocity of the air

cs cross section
wp wetted perimeter

Superscripts

– (overbar) average

Chapter 1

INTRODUCTION

Convective heat transfer in channels has many engineering applications, for instance, plate heat exchangers, solar collectors, heat dissipation from electronic equipment etc. Depending on the driving forces, the channel heat transfer can be divided into three types: natural convection, forced convection and mixed convection. The flow in natural convection is driven by buoyancy. Practical applications of this type of heat transfer can be found in solar collectors, fruit dryers. In forced convection, flow is driven by an external pumping force and has applications in many heat exchangers. Mixed convection is experienced when both natural and forced convection are present.

In engineering applications, especially in heat exchanger design, augmentation of heat transfer coefficient is very necessary. One of the important ways to augment heat transfer rate is to change the flow geometry with fins or corrugated surfaces. This increases heat transfer surface area compared to a flat heat transfer surface and also increases the heat transfer coefficient. However, the increase of heat transfer coefficient with these measures is usually at the expense of additional cost and pumping power except when flow is under pure natural convection.

There are a variety of thermal boundary conditions in practical channel flow applications. The typical thermal boundary condition could be either a uniform heat flux or a uniform wall temperature. In practice, the reality lies somewhere in between these two

extremes.

The problem considered herein is natural, forced and mixed convection heat transfer in a vertical cross-corrugated channel. The corrugated wall geometry was chosen because of the potential increase to the heat transfer rate. In this study, the channel is formed by two transversely positioned corrugated sheets and two flat side-walls which are thermally insulated. The thermal boundary condition is asymmetric and is defined in such a way that one sheet is being heated (in present study, with electric radiant heaters) and the other is thermally insulated.

The objective of this project is to study the heat transfer characteristics in this specific channel geometry and also develop heat transfer correlations for this problem. The application of this study includes solar collectors, heat exchangers, heat dissipation in electronic equipment etc.

Chapter 2

LITERATURE SURVEY

2.1 Natural convection

Natural convection is a common physical phenomenon. In the case of heating of most fluids in a vertical channel for instance, the density of the fluid inside the channel is decreased. Under the influence of a gravitational force, this difference of density between inside and outside a channel drives the fluid upwards. Simultaneously, the flow driven by the buoyancy force is being dragged downwards by the viscous force. By similarity consideration, this flow is usually described by Grashof Number Gr for a given fluid. Considering different fluids, Rayleigh number Ra is used in place of Grashof number. The movement of fluid is one of the key factors affecting the heat transfer coefficient. In natural convection, fluid movement is dependent on the heating condition at the wall. When the heating condition is set, the flow condition in the channel is also determined. Convective heat transfer is also related to the ratio of the heat dissipation and momentum dissipation of the fluid. The Prandtl number Pr , a physical property of the fluid, represents these effects. From the above, the heat transfer in a channel is determined for a given fluid under a given thermal boundary condition.

The convective heat transfer rate is usually compared with the pure conductive heat transfer rate for the working fluid. Nusselt number Nu is used to express this comparison. In natural convective heat transfer, this comparison is usually expressed through the

following dimensionless relation:

$$Nu = f(Gr) \quad (2.1)$$

for a given fluid. One of the objectives of this investigation is to experimentally determine the above relation in the cross-corrugated channel.

The overall range of natural convection heat transfer in vertical parallel plates includes three characteristic situations:

First, when the spacing between the plates is so large that each plate acts independently of the other, there is no interaction between the two plates either thermally or hydrodynamically. In this situation, a single plate limit is obtained. The single flat plate natural convection heat transfer has been well understood and documented in many heat transfer textbooks.

Second, when the two plates are very close to each other and this gap is much smaller than their length, a fully developed flow pattern inside the channel can be expected which is subject to the heating condition.

Between the above two extreme cases, a third situation, thermally developing region exists. In this situation, thermal and flow activities of the two plates are interacting with each other and the temperature profile is still developing in the channel.

The above three situations were characterized with specially defined Grashof number by Writz and Stulzman [1] in which the gap and length ratio of a channel b/L was taken

into consideration,

$$Gr = \frac{g\beta(T_w - T_\infty)b^3}{\nu^2} \frac{b}{L}. \quad (2.2)$$

Writz and Stulzman referred to the study by Aung et al. [2] and showed the flow regions characterized as follows with Grashof number defined above:

- 1000 < Gr : Single flat plate limit,
- 0.0 < Gr < 0.2 : Fully developed temperature profile,
- 0.2 < Gr < 1000 : Developing temperature profile.

The three characteristic situations are summarized in Table 2.1. The correlations in this table are taken from Eckert and Jackson [3], and Sparrow [4]. For the laminar flow in the single-plate situation, the two correlations in the table are slightly different from each other. The correlation for the developing flow situation was interpolated from the correlations for single-plate flow and fully developed flow situations and also applies for the latter two situations.

Natural convective heat transfer in vertical parallel plates has been extensively studied during the last half century. The most well known early investigator is Elenbaas. In his paper [5] published in 1942, he experimentally studied the heat dissipation by free convection in an open channel of parallel plates. The plates studied were heated symmetrically and maintained at a uniform temperature. He covered a range from a fully developed flow to a single plate limit. A numerical study with finite difference method of a similar problem was carried out by Bodia and Osterle [6]. They obtained good agreement with the experimental results of Elenbaas's except for the low values of Gr . Aung et al. [2] and Aung [7] studied the same problem as the one by Elenbaas except for the heating condition. The thermal boundary condition in their investigation was an asymmetric heating with either uniform heat flux or uniform wall temperature.

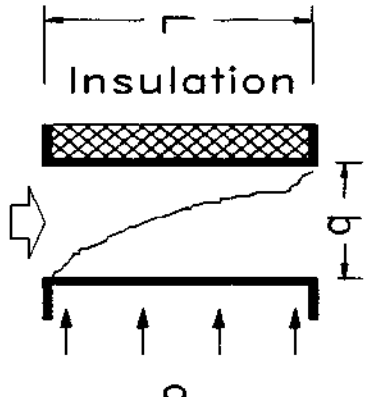
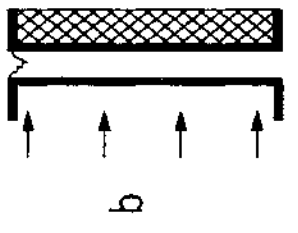
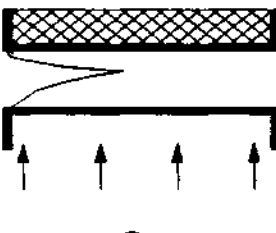
	<p><u>Single-plate flow situation:</u></p> <p>Turbulent: Eckert & Jackson [3]: $Nu_L = 0.0210(Gr_L Pr)^{0.4}$</p> <p>Laminar: Eckert & Jackson [3]: $Nu_L = 0.555(Gr_L Pr)^{0.25}$ Sparrow & Azevedo [4]: $Nu_b = 0.619(\frac{b}{L} Ra_b)^{0.25}$</p> <p><u>Fully developed flow situation :</u></p> <p>Laminar: Sparrow & Azevedo [4]: $Nu_b = \frac{1}{12}(\frac{b}{L}) Ra_b$</p>
	<p>Laminar: Sparrow & Azevedo [4]: $Nu_b = \frac{1}{12}(\frac{b}{L}) Ra_b$</p>
	<p><u>Developing flow situation :</u></p> <p>Laminar: Sparrow & Azevedo [4]: $Nu_b = \left\{ \left[\frac{1}{12} \left(\frac{b}{L} \right) Ra_b \right]^{-2} + \left[0.619 \left(\left(\frac{b}{L} \right) Ra_b \right)^{0.25} \right]^{-2} \right\}^{-0.5}$</p>

Table 2.1: Three characteristic natural convective flow situations.

The investigation covered both the fully developed flow situation and the developing flow situation for laminar free convection by numerical and experimental means.

Sparrow et al. [8] studied another asymmetric heating condition: one wall was heated at a uniform temperature, while the other wall was thermally insulated. A flow reversal was observed by flow visualization near the upper part of the unheated wall at Rayleigh numbers exceeding a threshold value. In a recent study by Sparrow [4], a range spanning between the fully developed flow situation and single plate boundary-layer situation was covered. Good agreement was shown between the experimental data and numerical results. A correlation covering the whole range of their experiment was obtained by using the method suggested by Churchill and Usagi [9]. The thermal boundary condition of Sparrow's work mentioned above [4] is quite similar to that of the present study and the results are used in comparison with the results from this study.

The studies mentioned above were conducted only for smooth flat plate channels. As far as the corrugated channel is concerned, there is very limited published work. In natural convection, laminar flow usually prevails and the laminar boundary layer is quite thick, and the surface roughness usually has no significant effect on the heat transfer. Large roughness also increases friction effects and decreases the flow rate, which results in a decrease of heat transfer rate. Faghri and Asako [10] numerically studied natural convection heat transfer in a channel with corrugated confining walls. A symmetric heating condition with uniform wall temperature was employed in their study.

Among the above mentioned studies, none deals with the developing flow situation in a corrugated channel. In this regime the flow boundary layers interact vigorously with each other due to development of the boundary layers and the flow pattern caused by

the corrugation of the channel.

2.2 Forced convection

In many practical applications, an external driving flow equipment like fan, pump etc. is used to enhance the heat transfer coefficient. Usually natural convection in this case is negligible compared with forced convection. There is rarely pure forced convection, however. Forced convection heat transfer refers to the case when forced convection dominates the heat transfer process, and the heat transfer relation is usually expressed as:

$$Nu = f(Re). \quad (2.3)$$

Corrugated-wall channel has been used and extensively studied to enhance heat transfer rate. It changes flow pattern, which results in an increase of heat transfer rate.

Goldstein and Sparrow [11] studied the transfer characteristics of a corrugated fin and tube heat exchanger configuration with heat-mass transfer analogy. It was noted that the windward or leeward orientation of the facets of the corrugated wall had a decisive effect on the transfer characteristics, with appreciably higher transfer rates prevailing on the windward facets. The average transfer coefficient due to the corrugated fin surface increased with Reynolds number. A study of the heat/mass transfer characteristics with the same analogy was reported [12]. The results showed that the average transfer coefficients for the corrugated channel were only moderately larger than those for a smooth parallel-plate channel in the laminar region. In the low Reynolds-number turbulent regime, the wall corrugations were responsible for an increase of nearly a factor of three in the average coefficient compared with the smooth wall channel.

Visualization of flow, made in a corrugated duct by O'Brien and Sparrow [13], revealed a highly complex flow pattern, including large zones of recirculation adjacent to the rearward-facing corrugation facets. From work done by Goldstein and Sparrow [11], the local transfer coefficient on the leeward facets is appreciably smaller than that on the windward. This might be explained from the flow recirculation on the leeward facets, which reduces the transfer dramatically.

Further detailed studies on the effect of rounding of the peaks of a corrugated-wall duct were accomplished by Sparrow and Hossfeld [14]. It is noted that rounding not only reduces the size of the separated region but also tends to diminish the general disturbance level of the flow, which leads to a reduction of the heat transfer coefficient. Sparrow and Comb [15] investigated the effect of interwall spacing and fluid flow inlet conditions. Molki [16] studied the effect of corrugation angle using a heat-mass transfer analogy. Kirpikov et al. [17] conducted an experimental study of the heat transfer and frictional resistance in a diverging-converging duct. The angles of successive expansion sections and contracting sections were varied. Geometrical parameters could dramatically change the heat transfer rate over a range of Reynolds number. In Kirpikov's subsequent paper [18], a configuration of the channel with a slant-orientated corrugation towards the flow was reported. It produced a three-dimensional alternating direction pressure gradient field, resulting in an increase of heat transfer coefficient.

Amano et al. [19] numerically examined turbulent flow and heat transfer characteristics in a corrugated-wall channel and the numerical results were compared with experiments. Asako et al. [20] conducted similar work in which the peaks of the corrugated wall were rounded. The rounding of the peaks resulted in a decrease of friction factor and Nusselt number, which agreed to the experimental results of Sparrow and Comb [15].

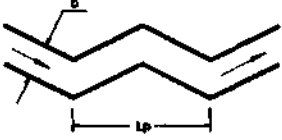
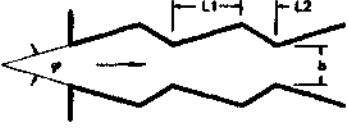
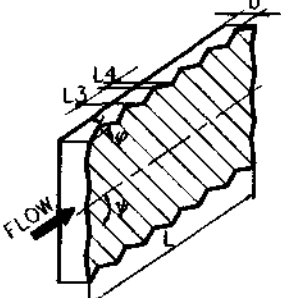
Channel Geometry	Correlation
	Sparrow & Comb [15]: $Nu = 0.416 Re^{0.634} Pr^{0.332}$ (Fully developed flow)
	Kirpikov et al. [17]: $Nu = 0.091 Re^{0.725}$ ($Pr = 0.7, b/L = 0.05, L1/L2 = 5, \varphi = 20^\circ$) $Nu = 0.030 Re^{0.79}$ ($Pr = 0.7, b/L = 0.05, L1/L2 = 1, \varphi = 8^\circ$)
	Kirpikov et al. [18]: $Nu = 0.0310 Re^{0.8}$ ($Pr = 0.7, b/L = 0.05, L3/L4 = 2, \varphi = 8^\circ 40', \psi = 45^\circ$)

Table 2.2: Some typical channel geometries and correlations.

Some typical and relevant channel geometries for forced convection have been summarized in Table 2.2.

Kirpikov et al. [17] showed that by adjusting the geometry parameters, the heat transfer for the first correlation is increased by 58.4% over the second correlation in a range of Reynolds number from 10,000 to 50,000. The channel geometry directly affect the flow pattern, which results in an increase of the heat transfer.

2.3 Mixed convection

When the pumping force is being superposed on the buoyancy force and the natural and forced convections are comparable, heat transfer is characterized as the combined natural and forced convection. Under the interaction of natural and forced convection, it is important to find an indication of the relative magnitudes of natural convection and forced convection effects.

In mixed convective flow over a vertical plate, a dimensionless group, (Gr_L/Re_L^2) , provides a measure of the ratio of buoyancy force to inertial force. Gr_L and Re_L are Grashof and Reynolds numbers based on the plate length. This criterion is used to delineate the following three flow regimes for a vertical flat plate:

$$\begin{aligned} (Gr_L/Re_L^2) >> 1: & \text{ 'Pure' natural convection,} \\ (Gr_L/Re_L^2) \approx 1: & \text{ Combined convection,} \\ (Gr_L/Re_L^2) << 1: & \text{ 'Pure' forced convection.} \end{aligned}$$

Metais and Eckert [21] studied various cases of convection in a vertical tube and showed that mixed convection exists when Gr_D is about 1. The Gr_D is diameter-based Grashof number and is defined as:

$$Gr_D = \frac{g\beta(T_w - \bar{T}_b)D^3}{\nu^2}, \quad (2.4)$$

where \bar{T}_b is the mean bulk temperature of the fluid. Their review showed that turbulent flow will exist if $Re_D > 2000$ and $Ra_D(D/L) < 5000$ or if $Re_D > 400$ and $Ra_D(D/L) > 5000$, where Ra_D is the Rayleigh number based on the diameter of the tube.

Mixed natural and forced convection between two vertical smooth parallel plates has been studied extensively. Quintiere and Mueller [22] presented an approximate analytical

solution to this problem with asymmetric and uniform thermal boundary condition, which means that each plate has either uniform wall temperature or uniform wall heat flux, but with different magnitudes. By using finite difference method, Dalbert [23] numerically investigated developing laminar flow with uniform but asymmetric heating boundary condition. A criterion based on:

$$Re^* = \frac{U_m b^2}{\nu L} \quad (2.5)$$

was also presented which delineated the following three zones:

$$\begin{aligned} Re^* < 1 &: && \text{a natural convection zone,} \\ 1 < Re^* < 300 &: && \text{a mixed convection zone,} \\ 300 < Re^* &: && \text{a forced convection zone.} \end{aligned}$$

The U_m is the mean velocity of the fluid and b, L are spacing and length of the parallel plates. The above criterion can be written as:

$$Re^* = \frac{U_m b^2}{\nu L} = Re_b \frac{b}{L}. \quad (2.6)$$

Re^* shows the effect of forced flow and it does not take any buoyancy effect into consideration. Using this criterion to indicate the relative effects of natural and forced convection is therefore not appropriate. Chato [24] included transition from laminar to turbulent flow problem in vertical channels and discussed the stability criterion below which the flow will be laminar for any disturbance. Hallman [25] experimentally observed transition from steady laminar to turbulent flow and detected turbulence by the temperature fluctuation of the heated surface wall. Baek et al. [26] reported a criterion marking the onset of the reversed flow and the transition from laminar to turbulent flow for combined convection in a vertical channel.

Studies on combined convection in a corrugated channel have been found by the present literature survey. Habachi and Acharya [27] numerically investigated laminar

combined convection in a partially blocked vertical channel. Flow separation and reattachment as well as recirculating eddies were shown after the blocked body, which might also occur in a corrugated channel at certain boundary conditions.

2.4 Scope of the present study

After the above survey of literature, It is noted that there has been no work done on the natural, forced and mixed convection in a cross-corrugated channel. This geometry channel may find applications in solar collector and heat exchangers. At this stage, an experimental approach was used to investigate the heat transfer characteristics and correlate heat transfer relations for natural, forced and mixed convection in a vertical cross-corrugated channel. In this study, one side of the channel is heated while the other is under an adiabatic condition.

Accordingly, an apparatus was designed and constructed. The results of the investigation will provide original data for engineers in the design of heat exchanger with this kind of channel geometry.

Chapter 3

EXPERIMENTAL APPARATUS

3.1 Experimental apparatus

In order to determine heat transfer relations in a cross-corrugated channel experimentally, an apparatus was constructed and is illustrated in Fig.3.1. The cross-corrugated channel was positioned vertically. The heating condition of the channel was asymmetric: the sheet with corrugation along vertical direction was heated with electric heaters, the other one was thermally insulated.

3.1.1 Corrugated sheets

For the purpose of practical application, commercial availability and low cost were considered first when choosing the material of the corrugated sheets. At last galvanized steel corrugated sheets were chosen. The corrugated sheet is of 30 gage (0.25 mm) thickness, 64.7 mm pitch and 12.7 mm from peak to valley. This kind of sheet has been widely used in construction industry for its simplicity and rigidity in structure. The profile of the corrugation can be approximately expressed as a sine function, which is shown in Fig.3.2. With the coordinates shown in Fig.3.2, the profile is expressed as

$$y = \frac{12.7}{2} \sin\left(\frac{2\pi}{64.7} x\right) \quad (3.7)$$

where x and y are in millimetres.

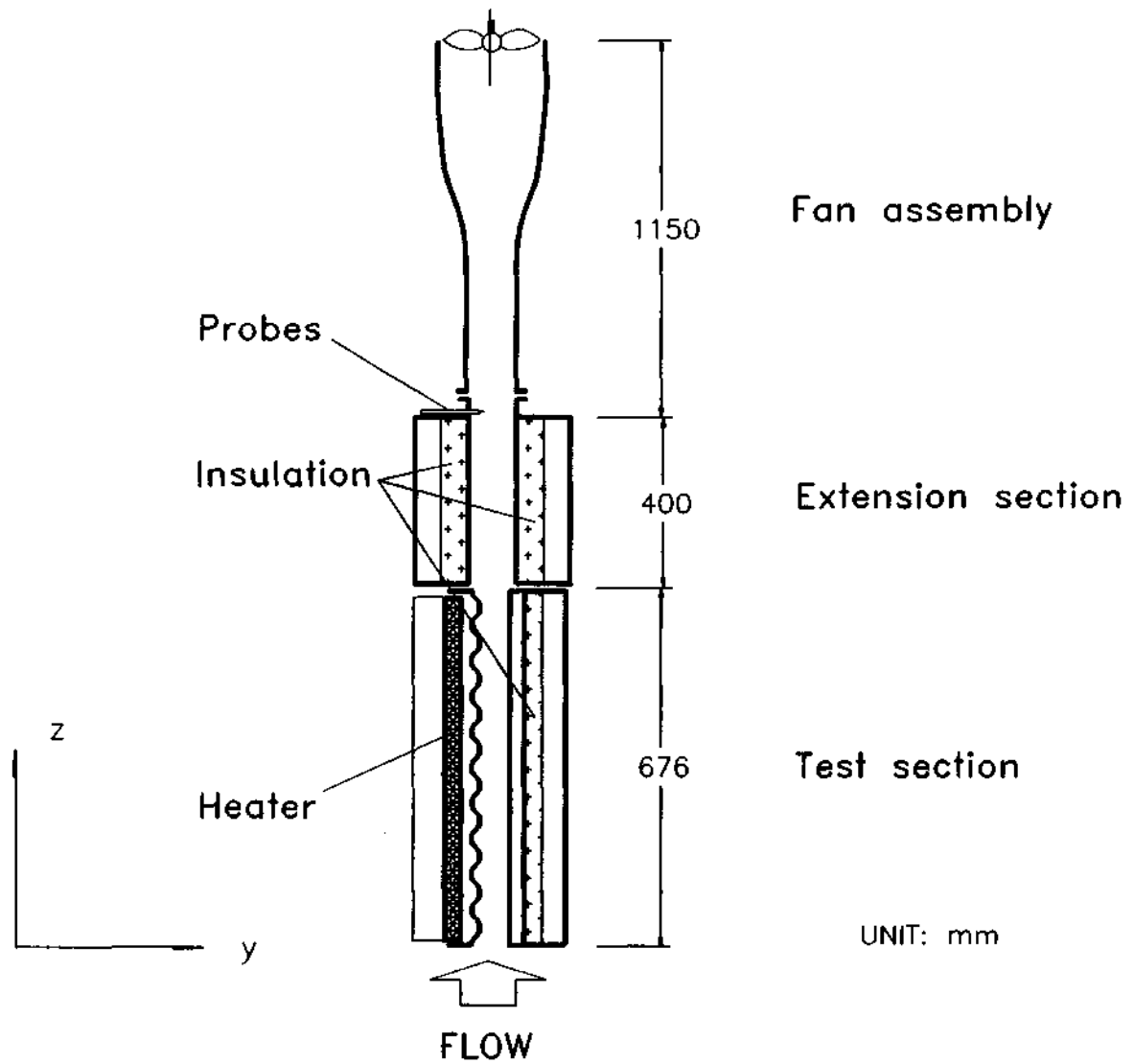


Figure 3.1: Schematic diagram of the experimental apparatus.

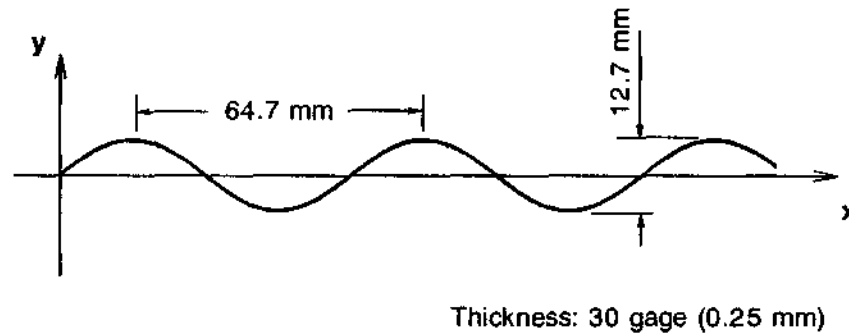


Figure 3.2: Profile of the corrugated sheet.

3.1.2 Working fluid

Air was chosen as the working fluid, as it is easily available and also makes the design of the experimental set-up easier than those using other fluids.

3.2 Test section and heating equipment

The vertical channel of the test section is formed by two transversely positioned corrugated sheets and two flat side walls. One of the corrugated sheets is heated with two electric radiant heaters. The other sheet is insulated with ceramic blankets. The two flat walls are thermally insulated with ceramic papers. Figure 3.3 shows the schematic diagram of the test section.

Dimensions of each heater are 641 mm in length, 213 mm in width and 491 mm in height. Each heater connects to 220 V a.c. power supply with adjustable voltage

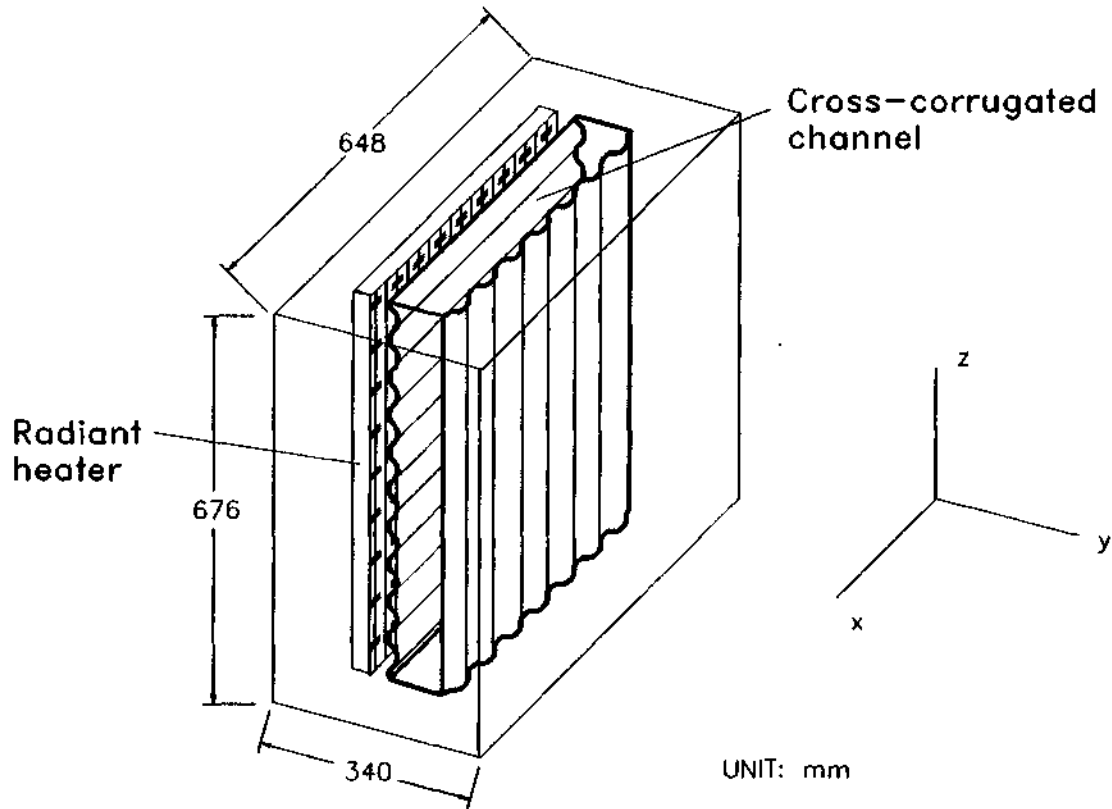


Figure 3.3: Schematic diagram of the test section.

control panel. The two identical heaters are positioned side by side. Therefore the heating surface area is 641 mm (length) by 426 mm (width), which confines the length and width of the test section channel. The dimension of the channel is 676 mm (10.4 pitches of the corrugation) in length, 438 mm (6.8 pitches) in width, with a variable channel gap.

In fluid dynamics, non-circular cross section flow is usually generalized with hydraulic diameter. The hydraulic diameter is defined as

$$D_h = \frac{4 \times A_{cs}}{L_{wp}}$$

for constant cross section channel. A_c denotes the cross section area of the channel and L_{wp} denotes the wetted perimeter.

For the cross corrugated channel configuration, the spacing is periodically varying, so is the cross-section area of the channel. Therefore the hydraulic diameter is defined as:

$$D_h = \frac{4V_{flow}}{A_{wetted}}, \quad (3.8)$$

where V_{flow} and A_{wetted} are the volume of the flow and the wetted area of the corrugated channel respectively. The concept of channel hydraulic gap b is also used in later heat transfer correlations and is defined as:

$$b = \frac{D_h}{2}. \quad (3.9)$$

In this cross-corrugated channel, the spacing between the two corrugated sheets is varying due to the corrugation. But minimum gap b_{min} and maximum gap b_{max} of the channel can be easily measured. The b_{min} is the minimum spacing between the two corrugated sheets and is the gap measured in the experiments. The b_{max} is the maximum spacing between the two corrugated sheets.

With the corrugation function Eq.(3.7) and the given channel dimensions, the hydraulic gap b of the channel is calculated against the minimum gap b_{min} . Figure 3.4 shows the relation between b and b_{min} . In Figure 3.4, the maximum spacing b_{max} between the two corrugated sheets is also shown.

3.2.1 Extension channel

In order to obtain the enthalpy flux in the channel, the temperature and velocity of the fluid before and after the channel have to be determined. Because of the complicated

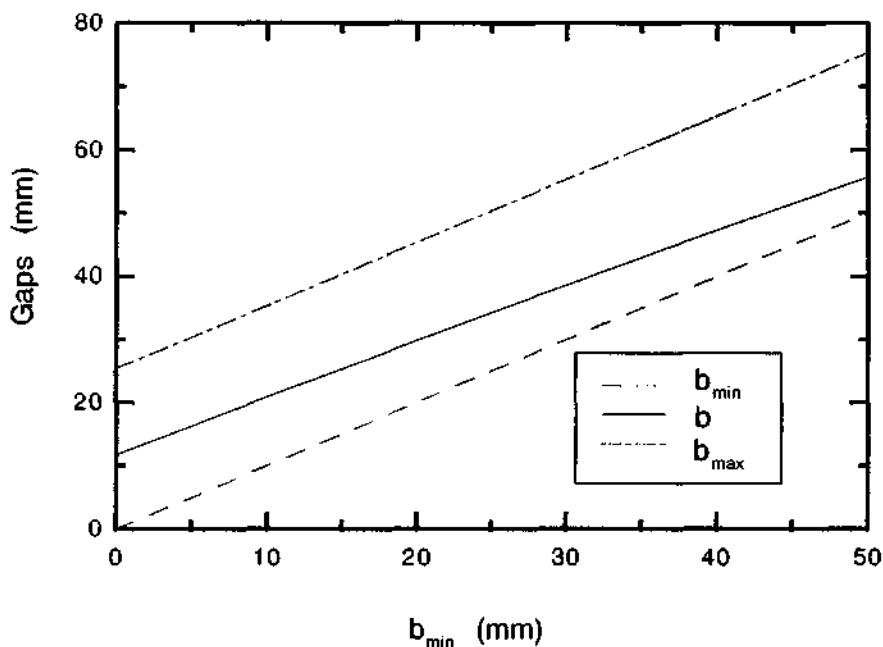


Figure 3.4: The channel hydraulic gap b and the minimum gap b_{min} .

geometry of the cross section and asymmetric heating condition of the test section, An insulated extension channel was placed on top of the test section, which mixed the fluid thermally and hydrodynamically before reaching the exit of the extension channel where the fluid velocity and temperature profiles were measured. The extension channel had rectangular cross-section geometry formed by four insulated flat walls. The dimensions of the extension channel were 400 mm length, 438 mm width and variable spacing subject to the setting of the test section spacing. The extension channel mixes the fluid both thermally and hydrodynamically before reaching the exit of the channel, where measurements are being taken.

3.2.2 Fan assembly

A 0.5 horsepower a.c. motor driven fan was used to suck the air from the top of the extension channel which provides the 'forced' flow condition. The motor speed was monitored by a variac. A 1150 mm long transition channel was used to connect a fan to the exit of the extension channel. This fan assembly provided forced flow conditions.

3.3 Measurements

3.3.1 Wall temperature measurement

Thirty gage J-type thermocouple was used to measure surface temperature of the heated corrugated sheet. The thermocouple wire was spot-welded on the sheets on the flow side and led out from the other side. Fig. 3.5 shows positions of the thermocouple wires on the heated corrugated sheet.

3.3.2 Wall heat flux measurement

Micro-foil heat flow sensors were used to measure local heat transfer rate across the heated surface of the corrugated sheet. In order to study the local heat transfer rate along the flow direction and compare the local heat transfer rates between the peak and the valley of the corrugation, four heat flow sensors were mounted on the peaks of the corrugation along the flow direction and one sensor was mounted on the valley of the corrugation. The sensors were fixed on the sheet of the flow side with high temperature resistant tape. Figure 3.5 also shows the position of the heat flow sensors.

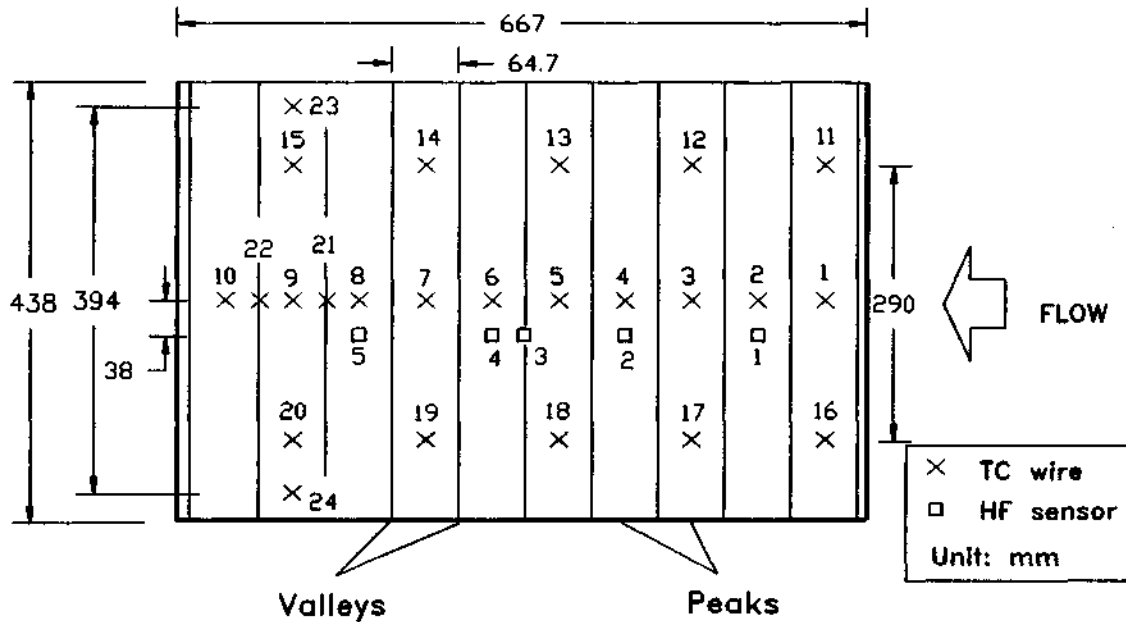


Figure 3.5: Position of thermocouple wires and heat flow sensors.

3.3.3 Pressure drop measurement

The static pressure drop along flow direction was studied by mounting three pressure taps on the side wall of the corrugated channel. Figure 3.6 shows position of the pressure taps. Pressure taps were connected to a multi-channel manometer in which alcohol was used as the pressure difference indicator between atmospheric pressure and the static pressure. The alcohol column was declined in 22° (the smallest declination angle obtained in this manometer) in order to increase accuracy of reading. The static pressure P was calculated from the following relation,

$$P_\infty - P = \rho_{Al} g \Delta h \quad (3.10)$$

where P_∞ is the atmospheric pressure, ρ_{Al} is the density of alcohol and Δh is the vertical height difference of the alcohol column between the column connected to the atmosphere

and the column connected to the pressure tap. The reading accuracy for h was ± 0.25 mm.

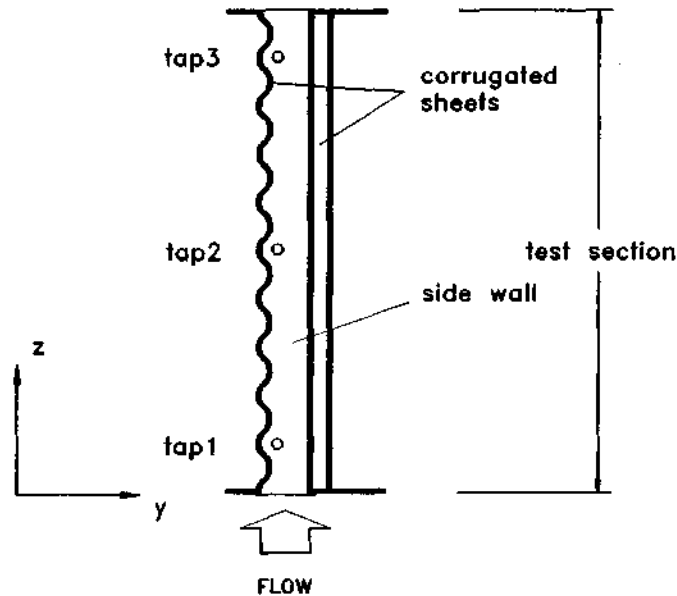


Figure 3.6: Position of pressure taps.

3.3.4 Air velocity and temperature measurements

The purpose of measuring the air velocity and temperature profiles is to obtain enthalpy flux of the working fluid across the vertical channel as well as the mean axial air velocity in the channel. The measurement was taken across the gap near the exit of the extension channel. A constant temperature hot-wire anemometer was used to measure the air velocity profile. A J-type thermocouple sensor was mounted together with the hot-wire probe to measure temperature profile. Positions of the hot-wire and thermocouple probes are illustrated in Fig.3.7.

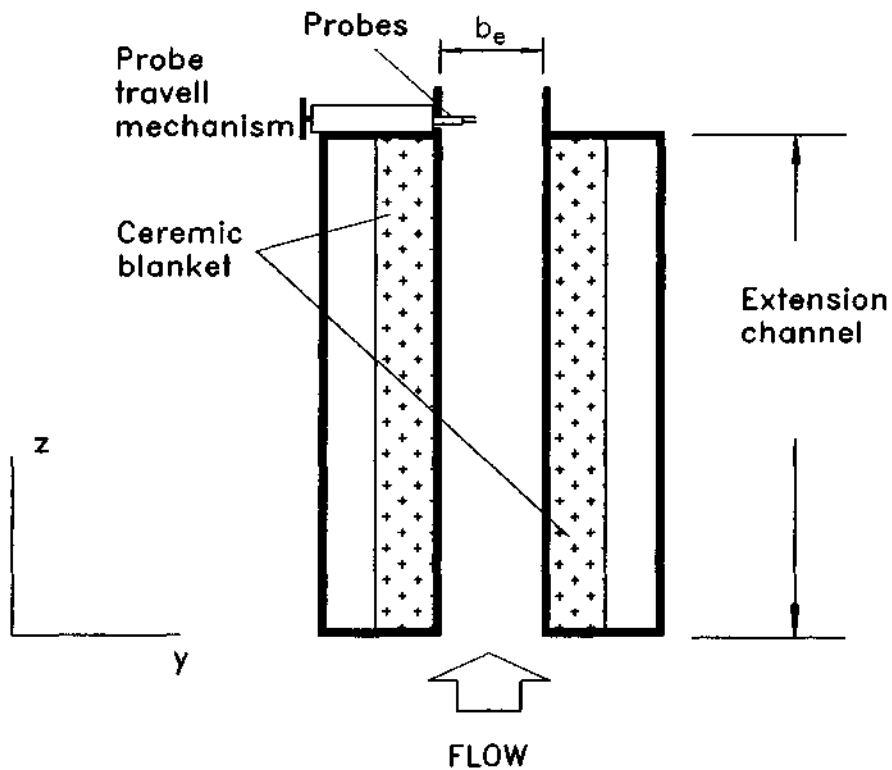


Figure 3.7: Position of hot-wire and thermocouple wire probes.

Since a high aspect ratio (gap width ratio of a channel) extension channel was used in the experiment, it was assumed that the flow at the cross-section of measurement was two dimensional. This assumption allows to measure velocity and temperature profiles at one plane at the exit of the extension section.

For a constant hot-wire anemometer, the velocity u is obtained through the use of the dimensionless expression,

$$Nu = C_1 + C_2(Re)^n, \quad (3.11)$$

where

$$Nu = \frac{E^2 R}{(R + R_3)lk\pi(T_{wire} - T_f)}, \quad (3.12)$$

and

$$Re = \frac{\rho u d}{\mu}. \quad (3.13)$$

The variables E and R are the sensor voltage and resistance, R_3 is the resistance of the fixed leg of the bridge and has a value of 40Ω , l is the length of the sensor, k is the thermal conductivity of the fluid, T_{wire} and T_f are the temperatures of the wire and fluid respectively. C_1 , C_2 and n are constants.

After choosing the sensor resistance R , The sensor temperature is also determined from:

$$R = R_{\infty}(1 + \gamma(T_{wire} - T_{\infty})), \quad (3.14)$$

where γ is the temperature coefficient of the wire resistance, R_{∞} is the resistance of the wire at the cold temperature T_{∞} of the wire. The cold temperature T_{∞} is the sensor temperature at the ambient condition, and the *cold* is relative to the *hot* operating temperature of the wire T_{wire} , which is elevated high above the ambient temperature. At calibration temperature, Eq.(3.11) can be simplified as:

$$E^2 = B_1 + B_2(u)^n, \quad (3.15)$$

where B_1 and B_2 are constants and are determined from a calibration curve, and n is an empirical constant and usually takes a value of about 0.5.

It might be important to emphasize that the calibrations were conducted at room temperatures. The fluid temperature at measurement was usually higher than room temperature because the fluid was heated before the measurement. A correction has to

be done when using the calibration curves. Here a method suggested by Kanevce and Oka [28] was used. In this method, the bridge voltage E is corrected by multiplying it by a correction factor. The corrected bridge voltage is expressed as:

$$E_c = E \left(\frac{T_{wire} - T_{cat}}{T_{wire} - T_f} \right)^{0.5}, \quad (3.16)$$

where T_{cat} is fluid temperature at calibration. The corrected bridge voltage E_c is used to predict air velocity with the calibration curve.

3.3.5 Data acquisition system

In order to obtain and process data, a computer data acquisition system was developed with a DT2801 board. The DT2801 board digitizes analog signals and takes commands from a data acquisition program in the PC computer. Signals from thermocouples and heat flux sensors are in millivolts, and they are amplified before putting into the DT2801 board. Figure 3.8 shows the schematic diagram of the system.

The data acquisition program written in C language communicates with the DT2801 board and also processes the data.

3.4 Calibration of instruments

Temperature measurements were made by using J-type thermocouples. The voltage across the thermocouple wires due to temperature difference between the two junctions is in an order of millivolts. Therefore this voltage signal first is put into the AD594C which is a monolithic thermocouple amplifier with cold junction compensation. Then the amplified signal is connected to the DT2801 data conversion board. The error through signal digitizing and data transfer is minimum compared to the accuracies of the sensor

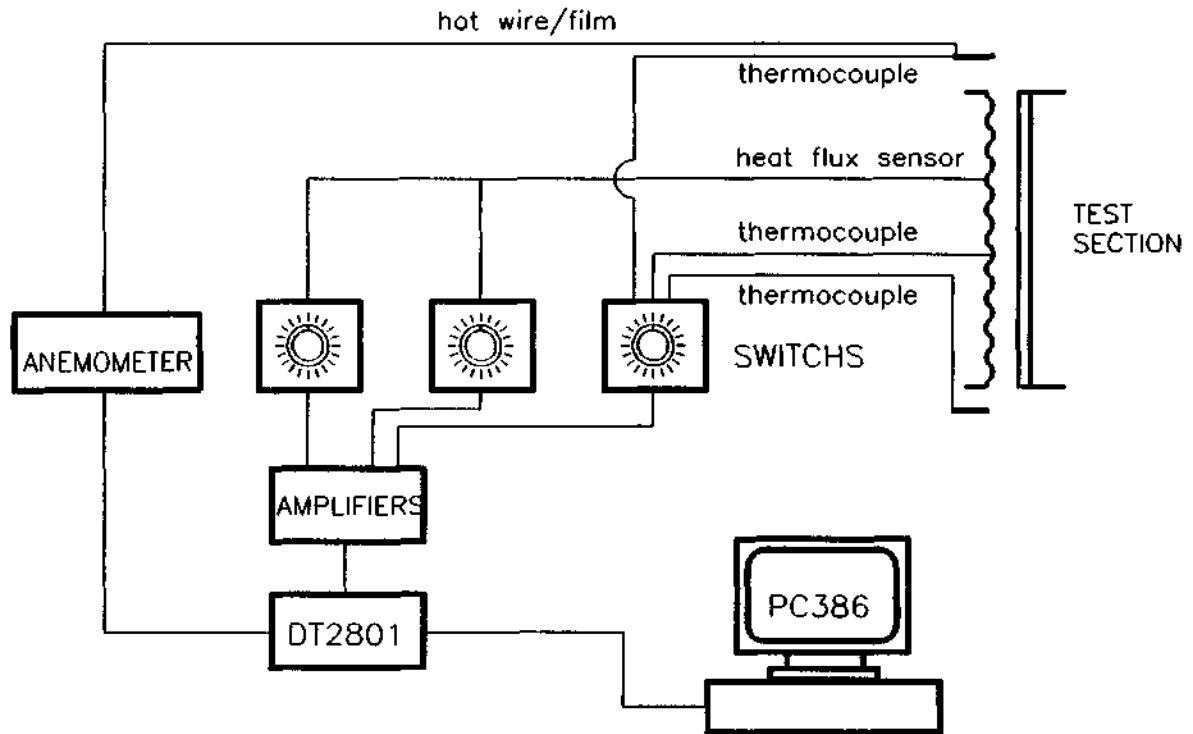


Figure 3.8: Schematic of data acquisition system.

and its amplifier. The calibration accuracy of AD594C amplifier is $\pm 1^\circ\text{C}$ [29].

Calibration for temperature measurement was made at the ice point and boiling point of water. The reading of temperature was within $\pm 1^\circ\text{C}$.

Local heat flux measurements were conducted with micro-foil heat flow sensors. Calibration of the sensors was provided by the manufacturer. Calibration was made at a surface temperature of 21°C . Table 3.3 shows calibrated output voltage for the sensors.

At any other surface temperature, the output of sensors has to be compensated by

Sensor No.	1	2	3	4	5
Output mV/(W/m ²)	1.850	1.913	1.884	1.871	1.846

Table 3.3: Output of heat flow sensors at surface temperature of 20°C.

multiplying an output multiplication factor. Figure 3.9 shows the multiplication factor vs. surface temperature. This correction curve was provided by the manufacturer and replotted here.

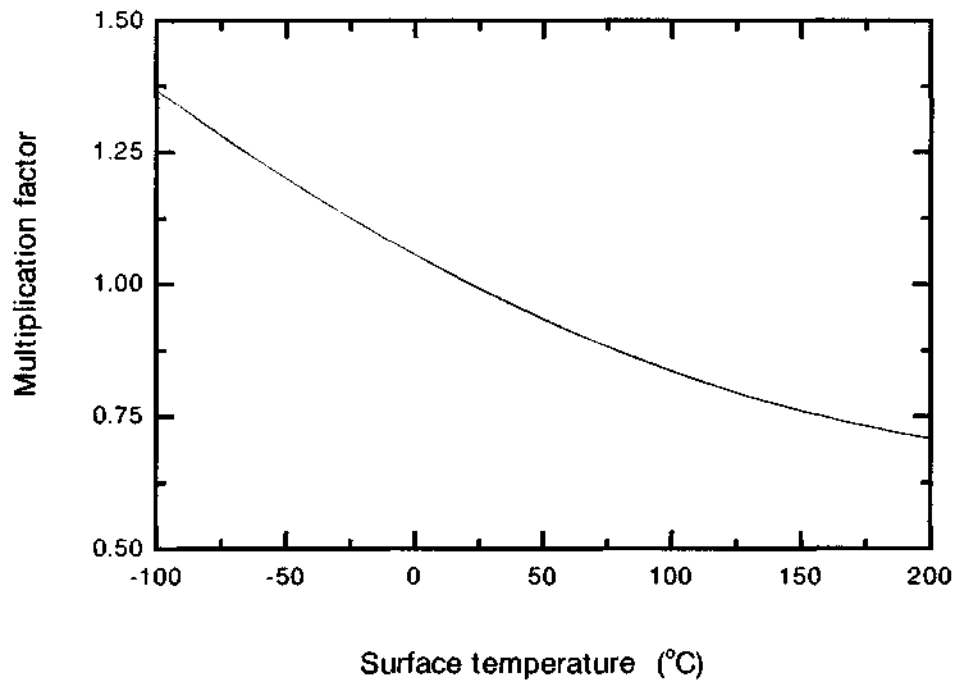


Figure 3.9: Output multiplication factor vs. surface temperature.

Accuracy of the output was not provided by the manufacturer, therefore error analysis in the heat flux measurement is not available. Since the local heat fluxes on the heated sheet measured with the sensors were not used in correlating the heat transfer

relations, the error would not affect the accuracy of the heat transfer relation in this work.

Velocity measurement of the fluid was performed with a TSI constant temperature anemometer [30]. A hot-film and a hot-wire probes have been used (the hot-film is termed as probe1 and the hot-wire is termed as probe2). Fluid velocity measurement for the gap1 and gap2 were taken with probe1 and probe2 respectively. The gap1 and gap2 refer to the two channel gaps in the cross-corrugated channel for the present study. After the experiment for gap1, the probe1 was broken and the same model substitute was not available, so that the probe2 was chosen and used for the gap2 experiment. The specifications for the probes are listed in Table 3.4, which are extracted from [31, 32]

	Model	Material	d	l	γ
Probe1	TSI 1210-60 Hot Film	Platinum	152 μm	2.0 mm	0.0024/ $^{\circ}\text{C}$
Probe2	Dentec 55P01 Hot Wire	Tungsten	5 μm	1.25 mm	0.0036 / $^{\circ}\text{C}$

Table 3.4: Specifications of hot wire/film probes.

The calibrations were done with the blue wind tunnel in the aerodynamics laboratory at the University of British Columbia. The calibration conditions of the hot wire/film probes are listed in Table 3.5. The operating temperature of the sensor in the table was calculated from Eq.(3.14).

When calibrating the probe, the hot wire/film probe was positioned in the center part of the wind tunnel with the wire perpendicular to the flow. The bridge voltage of the anemometer was measured against the velocity predicted by a Pitot tube manometer. The Pitot tube probe was put in the center of the wind tunnel by the hot wire/film probe, where both probes were in a uniform velocity section of the wind tunnel. Alcohol

	R_{∞}	R	T_{wire}	T_{∞}
Probe1	5.85 Ω	8.19 Ω	185.9 $^{\circ}\text{C}$	19.2 $^{\circ}\text{C}$
Probe2	4.13 Ω	6.19 Ω	161.6 $^{\circ}\text{C}$	23.0 $^{\circ}\text{C}$

Table 3.5: Calibration conditions of the probes.

was used in the manometer and the air velocity predicted from the manometer is related by the following:

$$\frac{1}{2}\rho u^2 = \rho_{Al} g h, \quad (3.17)$$

where ρ_{Al} is the density of alcohol and h is the absolute vertical difference of alcohol column in the manometer which is connected to the Pitot tube.

Figure 3.10 shows the calibration curves for the probe1 and probe2. From least square regression, constants in Eq.(3.15) are obtained and listed in Table 3.6.

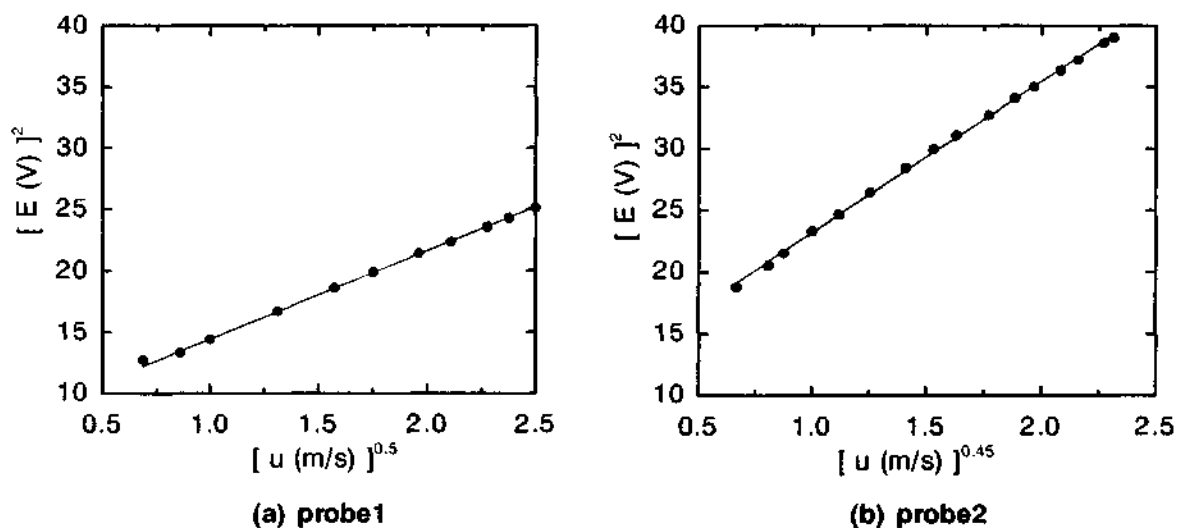


Figure 3.10: Calibration curves for hot wire/film probes.

	B_1	B_2	n
Probe1	7.285	7.172	0.50
Probe2	10.946	12.249	0.45

Table 3.6: Constants in Eq.(3.15).

The calibrations of the probes were performed in a velocity range of about 0.4 ~ 6.5 m/s. The lower limit of the velocity is confined by the limitation of the wind tunnel. The prediction of air velocity lower than 0.4 m/s (i.e. in natural convection case) is made by extrapolation of the calibration curve.

At a fluid temperature different from the calibration temperatures, Eq.(3.16) is used to correct the bridge voltage readings in order to compensate the temperature changes.

3.5 Experimental procedure

The experimental data were taken at steady states for all parameters. At first the data acquisition system, power supply to the heaters and power to the fan (in mixed and forced convection cases) were turned on. Then the voltage to the heaters and voltage to the fan were adjusted to preset the working condition, which needs some experience since setting the wall temperature and air velocity was required. Before starting data sampling, about 40 minutes were allowed to come to a steady state. The criterion used to determine steady state was that the wall temperature reading of the heated sheet did not change by more than 1 °C over a five minutes time interval. The wall temperature was checked after the data sampling.

The wall temperature readings were taken one by one by shifting the thermocouple positions with a thermocouple switch. The air temperature and velocity profile readings were then recorded at each position by moving the hot wire/film and thermocouple probes with a travelling mechanism. A dial gauge was mounted on the mechanism to determine the position of the probes. The wall surface heat flux readings were taken later for different positions with a switch.

After data sampling, the output data files from the data acquisition program were checked and the wall temperature was checked again to make sure that the system was still in a steady state.

An upper limit for the wall temperature to 150 °C was set for safety reason, since the extension channel is made of plywood and the suggested highest operating temperature for the bonding tape of heat flux sensor is 150 °C. The highest air velocity was limited to 6.0 m/s due to the limitation of the fan assembly.

Chapter 4

EXPERIMENTAL RESULTS AND DISCUSSIONS

Uniform wall temperature and uniform heat flux are two typical thermal boundary conditions in convective heat transfer. Experimental results show that the thermal boundary condition in this study is neither uniform heat flux nor uniform wall temperature. In presenting the experimental data, the heated wall temperature was averaged and heat transfer correlations were based on the uniform wall temperature boundary condition.

4.1 Calculations in the heat transfer correlations

Most of the heat transfer parameters in correlations are not directly measured. They are usually calculated through basic measurements, i.e. temperature, velocity etc. In this section, how the mean velocity U_0 , bulk temperature T_{b0} and heat transfer rate Q are calculated from our basic measurement will be described.

4.1.1 Mean velocity at the inlet of the channel U_0

The velocity profile is measured across the gap of the extension channel at the middle of the width of the thermally insulated extension channel. An assumption of two dimensional flow in the extension channel is made to simplify the measurement. The mean velocity at the end of the extension channel where the measurement was taken is

expressed as

$$U = \frac{1}{b_e} \int_0^{b_e} u \, dy, \quad (4.18)$$

where u is the local air velocity and it is a function of y , and b_e is the gap of the extension channel. The measurement of local velocity was taken with the hot-wire anemometer by travelling the probe discretely across the gap of the channel so that a numerical integration had to be carried out.

Mass conservation can be used to obtain the mean velocity U_0 at the inlet of the corrugated channel. For the corrugated channel, the spacing between the two corrugated sheets is not constant. The mean gap b_m of the channel is defined as:

$$b_m = \frac{b_{max} + b_{min}}{2}. \quad (4.19)$$

From mass conservation, we have

$$\rho_0 U_0 W b_m = \rho U W b_e, \quad (4.20)$$

where ρ_0 and ρ are evaluated at temperatures of T_∞ and T_{bo} respectively. The mean velocity U_0 at the inlet can be calculated from the above equation.

4.1.2 Bulk temperature of air at the outlet of the channel T_{bo}

To calculate the outlet bulk temperature, the temperature profile was also measured at the end of the thermally insulated extension channel. The bulk temperature of air at the outlet of the channel can be expressed as:

$$T_{bo} = \frac{1}{U b_e} \int_0^{b_e} u T \, dy, \quad (4.21)$$

where T is the local fluid temperature and is a function of y . Numerical calculation had to be performed since individual measurements were taken in the experiment.

4.1.3 Heat transfer rate Q

The heat transfer rate is the heating rate from the heated sheet to the fluid. Since the corrugated channel and extension channel are thermally insulated, the heat transfer rate equals to the enthalpy flux through the channel. The heat transfer rate can be expressed as:

$$Q = \rho c_p U W b_e (T_{bo} - T_{\infty}), \quad (4.22)$$

where ρ and c_p are evaluated at the outlet bulk temperature T_{bo} .

The detailed calculation procedure through a sample calculation is shown in Appendix A.

4.2 Results and discussions

Experiments were conducted for two channel gaps. Due to the complicated geometry of the channel, the heat transfer correlation is based on the channel hydraulic diameter D_h or the hydraulic diameter based channel gap b . Table 4.7 shows the channel gap related geometry parameters for the two channel gaps.

In order to use commonly accepted terminology and to compare with relevant work, the heat transfer parameters are defined at the beginning of each of the following sections.

	b_{min}	b_{max}	b_m	b	b_e	b/L
gap1 (mm)	44.8	70.2	57.5	51.4	70	0.0771
gap2 (mm)	18.4	43.5	31.1	28.4	44	0.0426

Table 4.7: Specifications of channel gaps.

4.2.1 Natural convection

In natural convection of a channel flow, Grashof number and Nusselt number can be defined either in terms of the channel gap or in terms of the channel length. In terms of the channel gap,

$$Gr_b = \frac{g\beta(\bar{T}_w - T_\infty)b^3}{\nu^2}, \quad (4.23)$$

$$Ra_b = Gr_b Pr, \quad (4.24)$$

$$Nu_b = \frac{Q}{LW(\bar{T}_w - T_\infty)} \frac{b}{k}. \quad (4.25)$$

In terms of the channel length,

$$Gr_L = \frac{g\beta(\bar{T}_w - T_\infty)L^3}{\nu^2}, \quad (4.26)$$

$$Ra_L = Gr_L Pr, \quad (4.27)$$

$$Nu_L = \frac{Q}{LW(\bar{T}_w - T_\infty)} \frac{L}{k}. \quad (4.28)$$

In natural convection, there is usually an appreciable variation between wall and free-stream temperatures and air properties are usually evaluated at film temperature. The film temperature is defined as:

$$T_{film} = \frac{\bar{T}_w + T_\infty}{2}. \quad (4.29)$$

It has been found over years studies that in natural convection that the heat transfer relation can be expressed in the following form for a variety of circumstances:

$$Nu = C(Gr Pr)^m = C(Ra)^m, \quad (4.30)$$

where C and m are constants determined experimentally. In this present experimental range, the Prandtl number of air was a constant. The heat transfer relation can also be written as Eq.(2.1) and it can only be used in a circumstance that the Prandtl number of the fluid is the same as the working fluid. But Eq.(4.30) is a more general form since it may be applicable to other different fluids.

Figure 4.11 shows the relation between Nu_b and Ra_b for gap1 and gap2. From this Figure, the most prominent observation is the slope m . From present correlation, m equals to 0.97 and 0.86 respectively for gap1 and gap2. In a smooth vertical channel, for the same range of Rayleigh number [33], heat transfer is in a single plate region and m takes a value of 0.25. This great difference might be one of the characteristics shown by our specially arranged cross-corrugated geometry of the channel.

From the work done by Sparrow and Azevedo [4], the slope m ranges from 1 to 0.25 from the fully developed region to the single plate region. Since this was a non-flat channel geometry, and hydraulic gap b was used as the channel gap, which is larger than the b_{min} , the flow boundary layer on the heated sheet may already interact with the other insulated sheet, and the flow is in a developing region, in which m takes a value between 0.25 and 1.

The heat transfer relation is also expressed with the channel length as the characteristic length and this is shown in Fig.4.12. Based on the experimental data of Sparrow

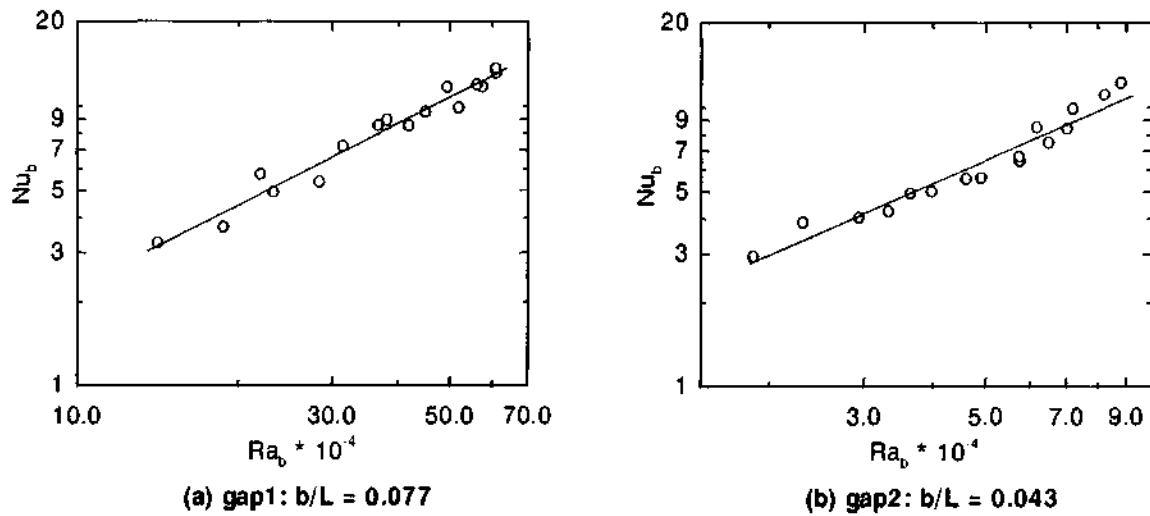


Figure 4.11: Relation between Nu_b and Ra_b in natural convection.

and Azevedo [4], present experimental data for the gap1 is still in the single plate limit region. The boundary layer on the heated sheet is still developing and it is not interacting with the other insulated sheet. The interesting feature is that for the gap2, the heat transfer coefficient is almost twice as much as that for gap1. Sparrow and Azevedo [4] conducted a similar experiment in a vertical flat plate channel with water as the heat transfer medium. The channel was bounded by an isothermal wall and an unheated insulated wall. Their typical results have also been plotted in Fig.4.12.

In general, heat transfer rate through channel flow will be decreased with a decrease of the channel gap in natural convection. Sparrow and Azevedo's results show that with the channel gap and length ratio b/L equal to 0.022, in a certain range of Rayleigh number Ra_L , the heat transfer rate is five percent larger compared to the larger channel gap (single flat plate region). This is contradictory to the general situation mentioned above. This phenomenon may be due to the interaction of the insulated wall to the developing boundary layer from the heated wall at certain smaller gap, which changes the flow

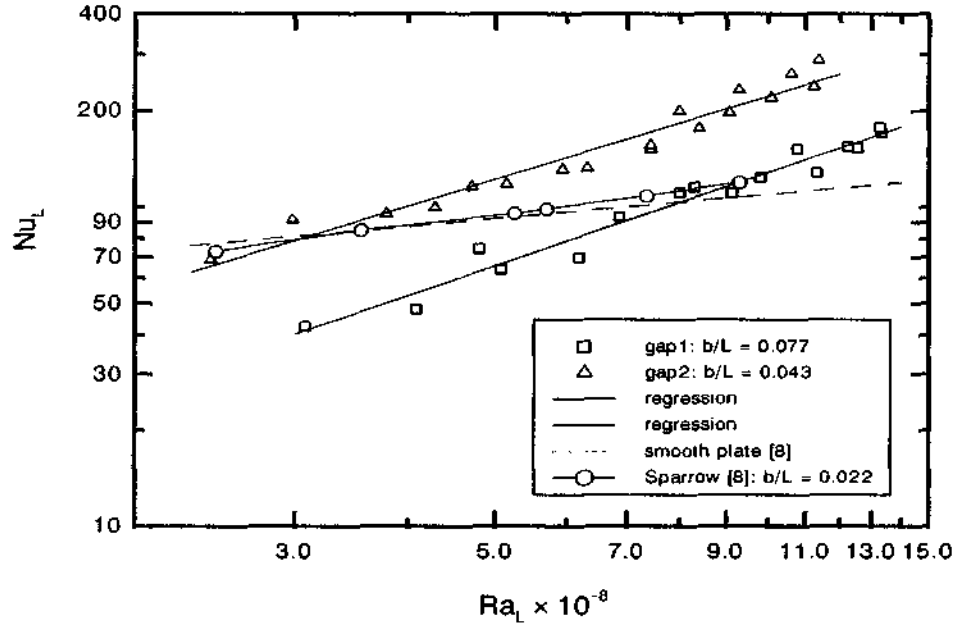


Figure 4.12: Relation between Nu_L and Ra_L in natural convection.

pattern of the single flat plate situation. The changed flow pattern leads to an increase of heat transfer coefficient, which exceeds to the heat transfer decrease caused by the decrease of the channel gap as in general cases.

The heat transfer relation for channel flow is generalized for different channel gaps in a single correlation expression:

$$Nu_b = C \left(Ra_b \frac{b}{L} \right)^m \quad (4.31)$$

where C and m are constants. This expression can be rewritten in another form:

$$Nu_L = C \left(\frac{b}{L} \right)^{4m-1} Ra_L^m = C_n Ra_L^m$$

For smooth vertical channel, the constant m ranges from 0.25 to 1.0. Therefore $(4m - 1)$ is always larger than or equals to zero. When the channel length L is fixed, a decrease of the channel gap b will results in a decrease of C_n except for fully developed flow situation in which m equals to 1. Simultaneously the constant m increases as the constant C_n decreases. The combined effects of the constants C_n and m will make the Nusselt number Nu_L decreases as the channel gap b decreases.

Present results showed that at smaller channel gap, the Nusselt number Nu_L was higher than that for the larger channel gap, which was also contradictory to the general cases mentioned above. The same explanation for smooth vertical channel flow also applies here. In this case a generalized correlation is not possible. for making such a correlation, further experiments with more channel gaps would have to be carried out, which was beyond the scope of this study.

4.2.2 Forced convection

In channel forced convective heat transfer, Reynolds number and Nusselt number are defined in terms of hydraulic diameter D_h :

$$Re_D = \frac{\rho U_0 D_h}{\mu}, \quad (4.32)$$

$$Nu_D = \frac{Q}{LW(\bar{T}_w - \bar{T}_b)} \frac{D_h}{k}. \quad (4.33)$$

Here the air properties are evaluated at mean bulk temperature \bar{T}_b . In this study, it is an arithmetic mean of air bulk temperature at the inlet and the outlet of the channel,

$$\bar{T}_b = \frac{T_{\infty} + T_{b\infty}}{2}. \quad (4.34)$$

Since the test section is vertical, there is always natural convection involved in the forced convection. Unfortunately there is no common criterion to determine when natural convection is negligible. In this work, when the natural convection effect was five percent of the forced convection or less in the heat transfer process, natural convection was considered negligible.

In order to achieve forced convective heat transfer conditions, a low heating input was used throughout the experiment. The experiments covered Reynolds number range from 3,000 to 50,000, which indicated turbulent flow.

Heat transfer relations in forced convection of channel flow are expressed as

$$Nu_D = C(Re_D)^m \quad (4.35)$$

where C and m are constants and are determined by experiment. The exponent m usually takes a value of 0.8 in most of turbulent forced convective heat transfer. Figure 4.13 shows the heat transfer correlation for gap1 and gap2. The values of m in this experiment are 0.90 and 0.81 for gap1 and gap2 respectively.

Figure 4.14 combines the results of both gap1 and gap2 together and compares with published results.

In the common range of Reynolds number for the two gaps, which is about 12000 to 21000, the heat transfer coefficient for gap1 is smaller than that for gap2. In general, Nusselt number based on the channel hydraulic diameter for a larger gap channel is higher than that for a smaller channel gap at the same Reynolds number. because the entrance effect is larger at larger gap. The local heat transfer coefficient is very large with

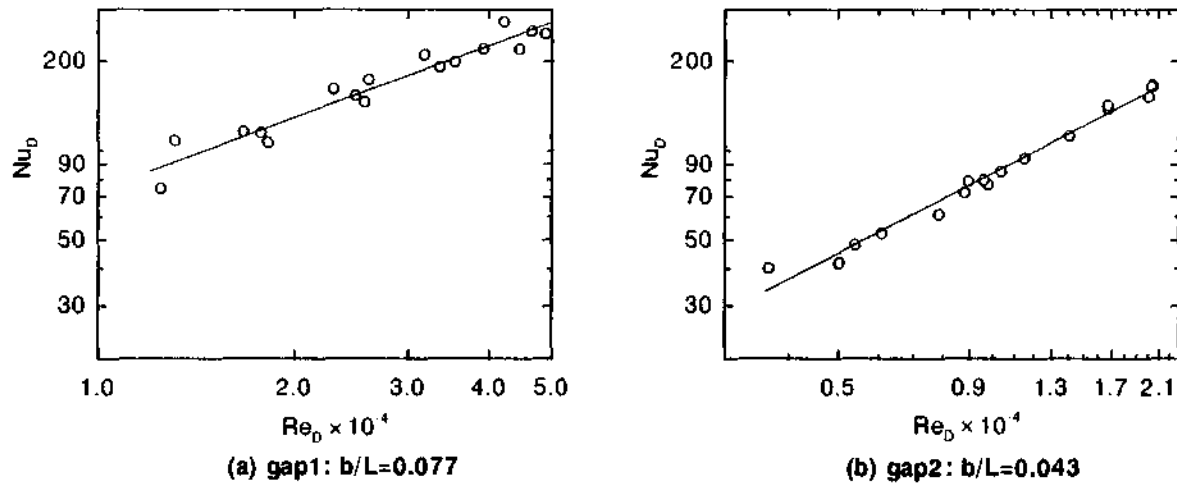


Figure 4.13: Heat transfer correlation for forced convection.

a flat velocity profile at the entrance, and it decreases along the channel to a constant value, which is the heat transfer coefficient for fully developed flow. This makes the average heat transfer coefficient higher for the larger gap length ratio channel than that for smaller gap length ratio. This is contradictory to the results of present experiments.

In this specific channel geometry, for gap1, the two corrugated sheets were farther apart compared to gap2. Each plate acted more or less independently. There was not as much interaction of the flow between the sheets as in the smaller gap. For gap2, the two sheets were close to each other. The flow interaction were more vigorous, which resulted in an increase of turbulence, as well as the heat transfer coefficient. The natural convection results also showed the same trend.

Present experimental results were correlated for a Re_D range of 3,000 to 50,000. In

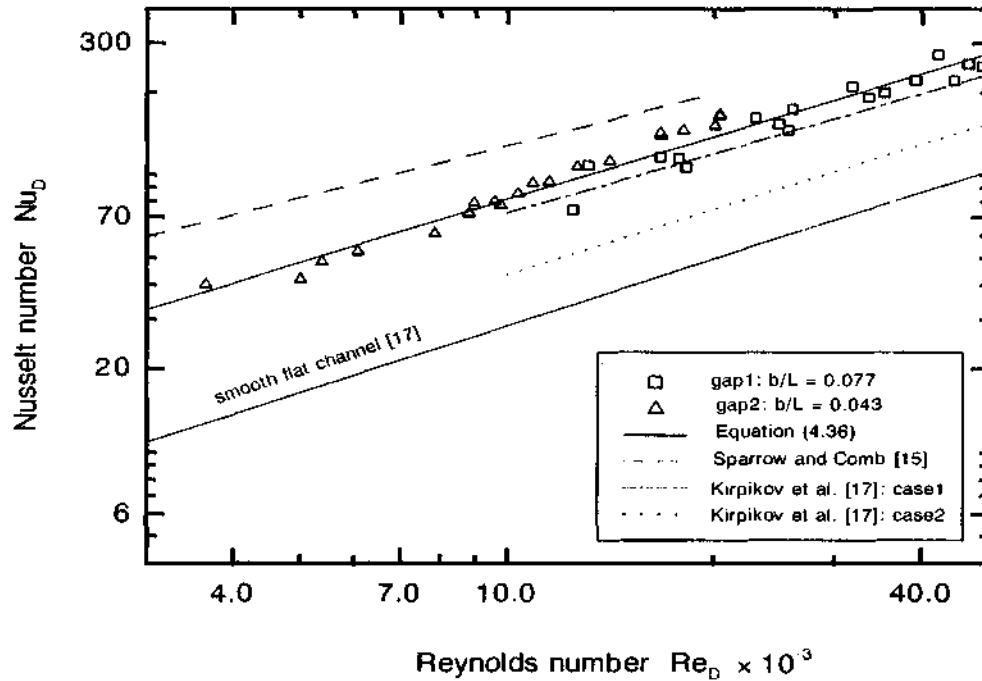


Figure 4.14: Relation between Nu_D and Re_D in forced convection.

this range, it was found that

$$Nu_D = 0.0743(Re_D)^{0.76}, \quad (4.36)$$

which is represented in Fig.4.14 as the solid line (regression).

Sparrow and Comb [15] correlated heat transfer relation in a corrugated channel with its geometry and dimensions shown in Table 2.2. The peaks and valleys of corrugation were sharp-edged. The effect of Prandtl number on heat transfer were studied and correlated in the following equation:

$$Nu_D = 0.416(Re_D)^{0.634} Pr^{0.332}. \quad (4.37)$$

The Prandtl number Pr of air in present experimental temperature range was 0.71. Using this Prandtl number in Eq.(4.37) gives a correlation which is replotted in Fig.4.14 for comparison.

Kirpikov et al. [16] conducted a similar experiment in a diverging-converging duct. The channel with its dimensions is shown in Table 2.2. Among their three experimental gaps, the one with gap length ratio equal to 0.05 was closest to present experimental gap settings. Kirpikov et al. obtained the best heat transfer coefficient when φ was 20° and the $L3/L4$ ratio was 5:1 among their three φ and three $L3/L4$ settings. This setting is termed as case1. The correlation of this result is:

$$Nu_D = 0.091(Re_D)^{0.725}. \quad (4.38)$$

Here the equivalent diameter of the inlet section of the divergent duct was used in correlations. At the setting of $\varphi = 8^\circ$ and $L3/L4 = 1:1$, the heat transfer rate was very poor, and it was termed as case2. The correlation for case2 was given by

$$Nu_D = 0.030(Re_D)^{0.79}. \quad (4.39)$$

These two cases and also the heat transfer for a constant cross section channel ($Nu_D = 0.018(Re_D)^{0.8}$) are replotted in Fig.4.14 for purpose of comparison.

The results of present experiments are compared with the above mentioned two studies in the common range of Reynolds numbers ranging from 10,000 to 50,000 based on correlation equations, and are summarized in Table 4.8.

In the comparison range, the heat transfer in Sparrow and Comb's study was about 42% higher than that in the cross-corrugated channel. The heat transfer in the cross-corrugated channel was about 16% and 83% higher compared to the case1 and case2

Nu_D	$Re_D = 10000$	$Re_D = 50000$
our correlation: Eq.(4.36)	81.5	276.8
Sparrow and Comb [15]	127.6	353.9
Kirpikov et al.[17]: case1	72.3	232.2
Kirpikov et al.[17]: case2	43.4	154.6
constant cross section [17]	28.5	103.4

Table 4.8: Comparison of Nusselt number Nu .

respectively of Kirpikov's investigation. From Table 4.8, it can be seen that by choosing proper configuration parameters, the heat transfer coefficient can be increased substantially.

4.2.3 Mixed convection

In mixed convection, natural convection and forced convection are comparable. The heat transfer relation is expressed as:

$$Nu = f(Re, Gr). \quad (4.40)$$

Several different temperatures have been used to evaluate fluid properties in different circumstances, i.e. film temperature, wall temperature, bulk mean temperature and local bulk temperature [34]. In this experiment, air was used as working fluid and the wall temperature and the free-stream temperature were appreciably different. In such a situation, film temperature was recommended for evaluation of the fluid properties [35]. Therefore the film temperature was used to evaluate the fluid properties in correlation of this experimental relation. Reynolds number, Grashof number and Nusselt number are defined as follows:

$$Re_D = \frac{\rho U_0 D_h}{\mu}, \quad (4.41)$$

$$Gr_D = \frac{g\beta(\bar{T}_w - \bar{T}_b)D_h^3}{\nu^2}, \quad (4.42)$$

$$Nu_D = \frac{Q}{LW(\bar{T}_w - \bar{T}_b)} \frac{D_h}{k}. \quad (4.43)$$

The mixed convection correlation is presented by comparing with 'pure' forced convection. In order to keep the comparison consistent, correlations for forced convection were made with air properties evaluated at the film temperature. Eq.(4.44) and Eq.(4.45) show the correlations for 'pure' forced convection with properties evaluated at film temperatures for gap1 and gap2 respectively:

$$Nu_F = 0.0274(Re_D)^{0.853}, \quad (4.44)$$

$$Nu_F = 0.0145(Re_D)^{0.94}, \quad (4.45)$$

where Nu_F and Re_D are hydraulic diameter based Nusselt number and Reynolds number for forced convection

Jackson and Hall [36] derived a criterion for the onset of buoyancy effects in a heated vertical tube with turbulent flow in the upward direction. With an approximate analysis of the reduction of the shear stress near the wall due to the buoyancy effect, it was found that the Grashof number and Reynolds number combine together in the form $\overline{Gr}/Re^{2.7}$ to control the extent to which buoyancy forces modify the shear stress. Through chain relations among shear stress, friction coefficient, Reynolds number and Nusselt number, the Nusselt number in mixed convection is related to the Nusselt number for 'pure' forced convection and the above mentioned criterion $\overline{Gr}/Re^{2.7}$. The Grashof number \overline{Gr} is defined with the density difference instead of temperature difference:

$$\overline{Gr} = \frac{(\rho_b - \bar{\rho})D^3g}{\rho\nu^2}, \quad (4.46)$$

where D is the tube diameter, ρ_b is the fluid density evaluated at the bulk temperature T_b and $\bar{\rho}$ is an integrated density,

$$\bar{\rho} = \frac{1}{T_w - T_b} \int_{T_b}^{T_w} \rho \, dT. \quad (4.47)$$

The Grashof number defined with the density difference is different from that defined with the temperature difference at the beginning of this section. Aung [34] derived the relation between the two Grashof numbers with certain approximations, which gave

$$\overline{Gr} \approx \frac{Gr_D}{2}. \quad (4.48)$$

In present experiments, it was difficult to fix either Grashof number or Reynolds number with one of the two parameters changed. Therefore no correlation was made between Nusselt number and Grashof number with fixed Reynolds number or Reynolds number with fixed Grashof number. The experimental results are correlated in the following form:

$$\frac{Nu_D}{Nu_F} = f \left(\frac{Gr_D}{Re_D^{2.7}} \right). \quad (4.49)$$

The mixed convection experiment was conducted by adjusting both heating rate (changing the voltage) and fan speed in order to have both natural and forced convection effects at a comparable magnitude. This was a buoyancy-aided flow. The experiment covered a range of Reynolds number from 3,000 to 44,000 and a range of Grashof number from 2.3×10^5 to 65×10^5 . This falls into the turbulent flow region. The Nusselt number is normalized with Nusselt number for 'pure' forced convection and expressed as a function of $Gr_D/Re_D^{2.7}$. Figure 4.15 shows this relation obtained from the present experimental data.

From Fig. 4.15, three regions can be defined. First, when $Gr_D/Re_D^{2.7} < 2 \times 10^{-6}$, the Nu_D/Nu_F is equal to about 1 and the forced convection prevails. Second, when

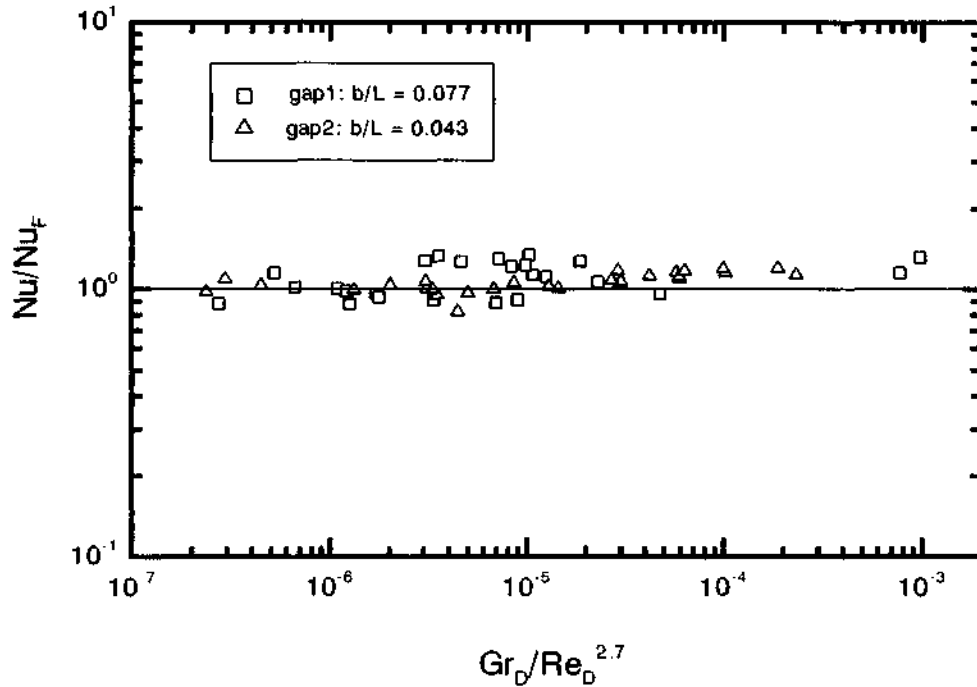


Figure 4.15: Heat transfer relation for mixed convection.

$Gr_D/Re_D^{2.7} > 2 \times 10^{-5}$, the ratio Nu_D/Nu_F deviates from 1 and increases, and the natural convection effect increases. Third, between these two regions, the ratios Nu_D/Nu_F were scattered. In this region, the heat transfer is supposed to be less than the pure forced convection, since the fluid close to the heated wall experiences a buoyancy force in the same direction of motion, which tends to decrease the shear stress and results in laminarization of the fluid flow [36]. For gap2 in Fig. 4.15, the experimental data agree with the above analysis, but for gap1, the data were much more scattered and the impairment of heat transfer is not observed. In the second region, the heat transfer recovers from impairment at high Grashof numbers, since the shear stress changes sign and energy inputs to the turbulent motion increase [34]. From Fig. 4.15, the criterion

for the onset of buoyancy-induced impairment of heat transfer can be obtained from the limit:

$$\frac{Gr_D}{Re_D^{2.7}} \leq 2 \times 10^{-6}. \quad (4.50)$$

Jackson and Hall [36] presented the criterion through an approximate analysis as follows:

$$\frac{\overline{Gr}}{Re^{2.7}} \leq 10^{-5}. \quad (4.51)$$

The difference between these two criteria comes from first, the definitions of the two Grashof numbers ($\overline{Gr} \approx 0.5Gr_D$), and second, from neglecting the Prandtl number effect. Taking these factors into consideration, the two criteria will match even better though they are already in the same order of magnitude.

In general, the mixed convective heat transfer coefficient had no significant difference from the 'pure' forced convective heat transfer coefficient.

4.2.4 Pressure drop and friction factor

Fluid static pressure in a channel flow decreases along the flow direction due to the friction between the fluid and the channel wall. A study on the subject in the cross-corrugated channel was conducted under forced convection condition.

The difference between atmospheric pressure and the static pressure drop along the flow direction was measured with pressure taps mounted on the side wall of the corrugated channel. The pressure taps were placed on the side wall instead of the corrugated surface due to the difficulty of mounting the pressure taps on the heated and thin sheet. Therefore the pressure measured with the taps was an approximation of the pressure on the corrugated surface. Figure 4.16 shows axial pressure distribution. From the figure,

we can see that the pressure at the inlet of the corrugated channel has jumped since the pressure drop should be zero at the $z/D_h = 0$ point. This pressure jump was due to the fluid flow inlet condition or say, entrance effect.

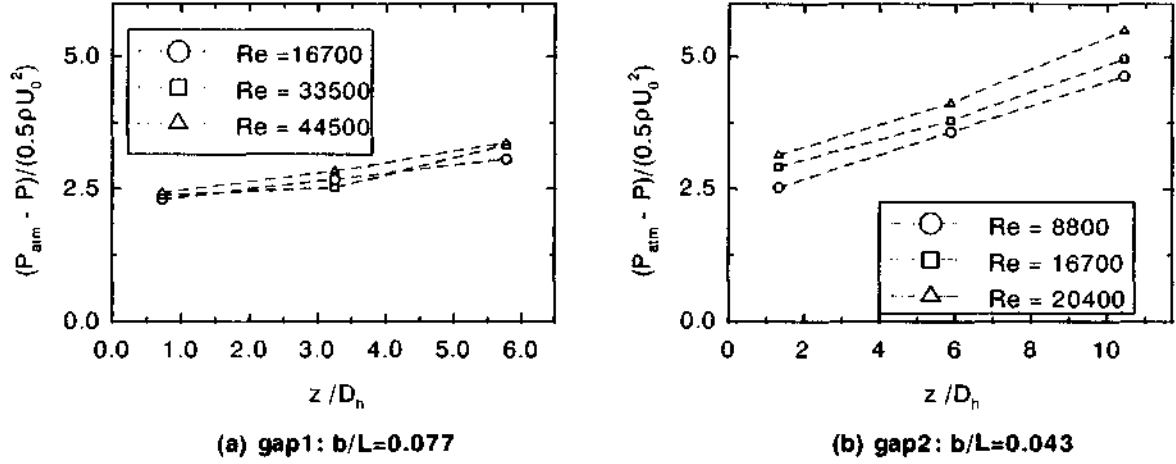


Figure 4.16: Axial pressure distribution in the corrugated channel.

The friction factor ξ is defined as:

$$\xi = \frac{-dP/dz}{\frac{1}{2}\rho U_0^2} D_h, \quad (4.52)$$

where P is static pressure of the fluid in the corrugated channel. The three pressure taps gave an approximate linear change of pressure along the channel, which meant the fluid flow was already fully developed before the pressure tap1. The slope in Fig. 4.16 represents the friction factor. In our situation the fully developed friction factor can be derived from Eq.(4.52) and written as:

$$\xi = \frac{-(P_3 - P_1)/(z_3 - z_1)}{\frac{1}{2}\rho U_0^2} D_h, \quad (4.53)$$

where P_1 and P_3 are pressure readings from tap1 and tap3 respectively and z_1 and z_3 correspond to the tap1 and tap3 positions in the z coordinate.

Figure 4.17 shows the variation of the friction factor ξ with Reynolds number Re_D . In general, friction factor in a channel flow decreases with Reynolds number. The friction factor increases with channel roughness and its decrease with Reynolds number tends to ease with the increase of relative roughness of the channel, which is shown by the famous Moody Chart [33]. From Fig.4.17, the friction factor is almost constant in our Reynolds number range, which corresponds to a channel with a very rough surface.

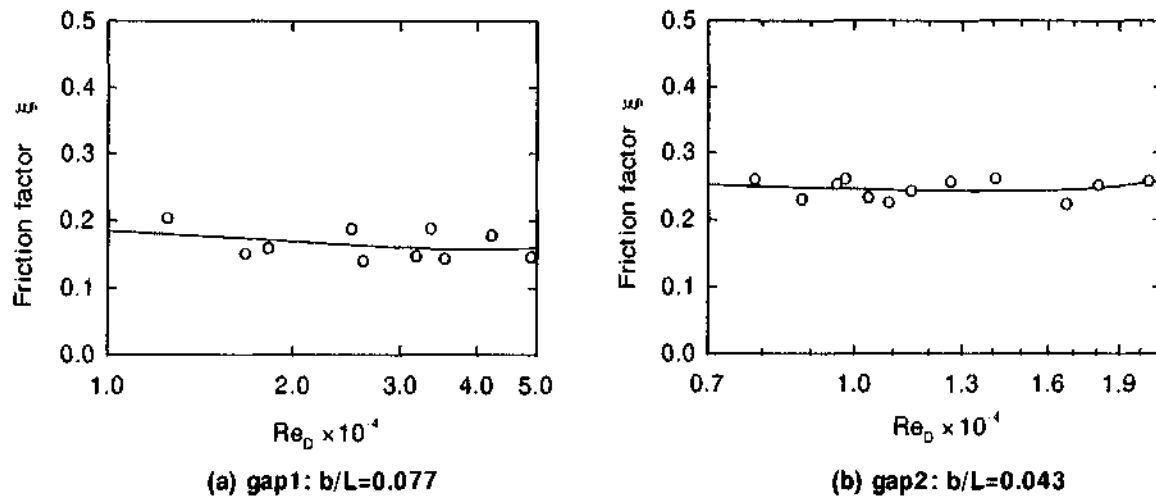


Figure 4.17: Relation between friction factor ξ and Re_D .

In this experiment, the friction factor ξ ranged from 0.14 to 0.27. The friction factor ξ in the study of Kirpikov et al. [17] in the same range of Reynolds number is listed below:

	$Re_D = 3.0 \times 10^3$	$Re_D = 5.0 \times 10^4$
Kirpikov et al. [17]: case1:	0.12	0.086
Kirpikov et al. [17]: case2:	0.046	0.028

The friction factor above was very small, i.e. the friction factor in the case2 was

comparable to the friction factor in a pipe with a relative roughness of 0.004. Sparrow and Comb [15] showed quite high fully developed friction factors ranging from 1.22 to 1.39 in a range of Reynolds number from about 2000 to 20000.

From comparison of heat transfer and friction factor with Kirpikov's and Sparrow's results, it is confirmed that the increase of heat transfer is usually accompanied with an increase of friction factor, which means at an expense of pumping power.

4.2.5 Local heat transfer rate on the heated wall

The fluid flow pattern in the corrugated channel directly affects the heat transfer coefficient in a convective heat transfer, and results in a change of the local heat transfer rate in a non-uniform heat flux condition like in this experiment. In a corrugated channel, the fluid flow has a general change along the flow direction and also has a periodic change along the corrugation. A study on this subject was conducted under a forced convection condition.

The local heat transfer rate q across the heated corrugated sheet was measured with micro-foil heat flow sensors. Figure 4.18 shows the local heat flux change along the flow direction at some fixed Reynolds numbers. In this figure, the readings of those sensors at the peaks of the corrugated sheet are connected with lines.

At a uniform heat flux condition, the local heat transfer rate is constant along the flow direction. At a uniform wall temperature condition, the local heat transfer rate decreases along the flow direction. The local heat flow rate q in this study showed an

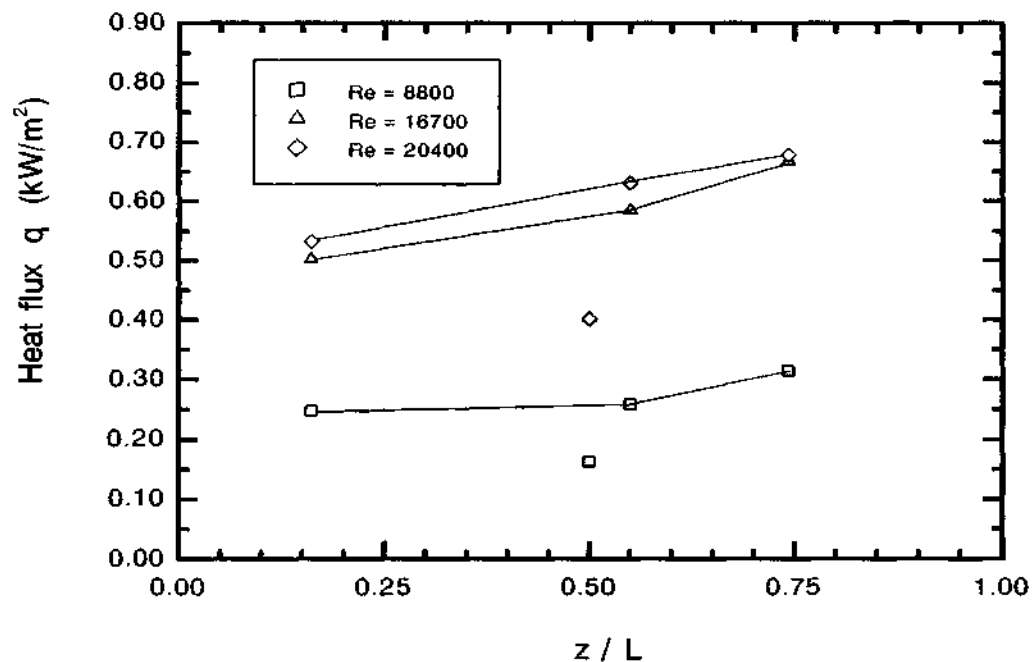


Figure 4.18: Local heat flow rate along the flow direction.

increase along the flow direction at the measurement range, which meant that the thermal boundary condition of this study was neither a uniform heat flux nor a uniform wall temperature. In Figure 4.18, it can be noted that the local heat flux at the peak (No.4 sensor reading) was larger than that at the valley (No.3 sensor reading). The local heat transfer coefficient at the peak was also higher than that at the valley, since the local wall temperature at the valley was higher than that at the peaks. Local wall temperature measurement showed that wall temperature at the valley was usually higher than that at the neighboring peaks. This was due to the higher local heat transfer coefficient at the peaks explained above. In this study, the measurement was taken only on peaks and a single valley of the corrugation. It is still unknown how the local heat transfer coefficient changes along the corrugation. Goldstein and Sparrow [11] found that the local

heat transfer coefficient on the leeward facets was appreciably smaller than that on the windward facets in a corrugated channel. From present study, a general change of local heat transfer coefficient along a corrugation may be described.

From analysis of the experimental data, it is noted that the local heat flux difference between peak and valley of the corrugated sheet has a certain relation with fluid velocity. The heat flow sensor No.3 was placed on the middle of the corrugated sheet and was also on the peak of a corrugation, and the sensor No.4 was half pitch after the sensor No.3 along the flow direction, which was on the valley of a corrugation. The heat fluxes q_3 and q_4 are the corresponding heat flux readings of the sensors No.3 and the No.4. The local heat flux ratio q_3/q_4 and Reynolds number has been correlated for gap2 and is shown in Fig.4.19.

At very low Reynolds numbers, this ratio was very low. The local heat transfer coefficient at the valley was much lower than that at the peak. The heat transfer mainly took place on the peak area. As the Reynolds number increased, this difference became less, and the heat transfer on the valley area became more and more active.

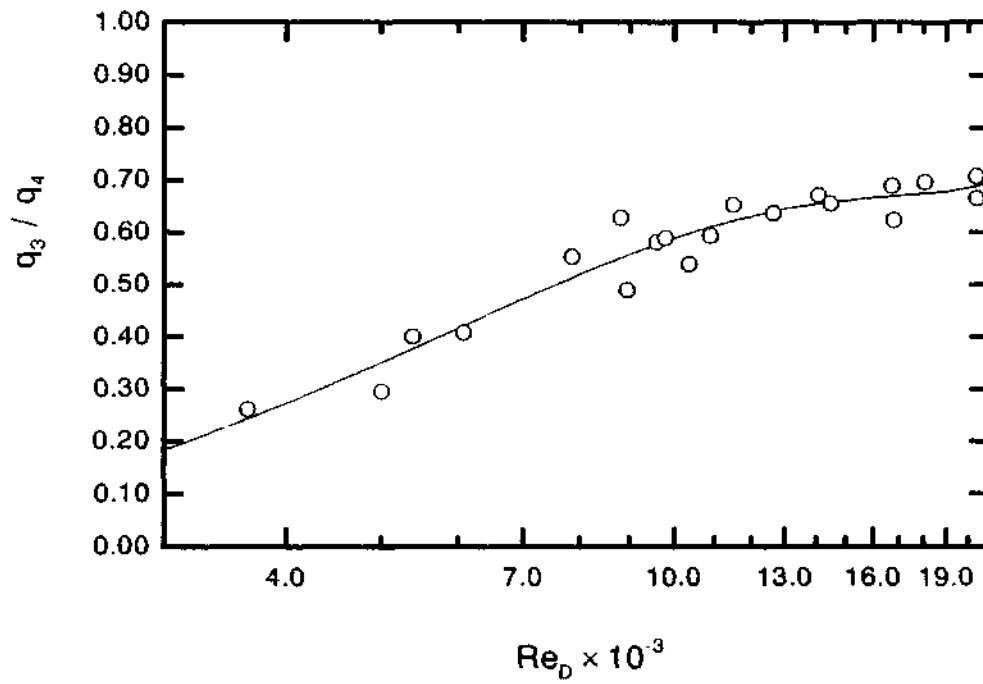


Figure 4.19: Local heat flux ratio variation with Re_D for gap2.

Chapter 5

CONCLUSIONS

Natural, forced and mixed convective heat transfer in a vertical cross-corrugated channel has been experimentally studied. The following conclusions may be drawn.

5.1 Natural convection

Natural convection shows significant different characteristics when it is compared to a smooth vertical channel at the same gap and length ratio. The slope m in Eq.(4.30) is very different from the smooth channel, which means that the flow starts interacting at smaller gap and length ratio in the cross-corrugated channel.

The channel length based Nusselt number Nu_L was larger at the smaller gap than at the larger gap in our two-gap experiment, which is contradictory to a common smooth channel natural convection. This phenomenon is also observed by Sparrow and Azevedo [4]. The significant difference shown in present experiments might be due to the vigorous interaction of the flow on the channel wall surface at this smaller gap.

5.2 Forced convection

Forced convective heat transfer was conducted for two gaps of the channel, and the correlation was made in a Reynolds number range from 3,000 to 50,000 as follows:

$$Nu_D = 0.0743 (Re_D)^{0.76}.$$

Pressure drop and friction factor were also correlated with the pressure taps mounted on the side wall of the channel. The pressure readings of the three pressure taps showed that the static pressure decreased approximately linearly along the flow direction and accordingly the variation of the fully developed friction factor with Reynolds number was observed. In this experimental range of Reynolds number, the friction factor ranged from 0.14 to 0.27.

Local heat flux measurement showed that the local heat transfer coefficient on the peak of the heated corrugated sheet was larger than that on the valley. The ratio of the local heat flux between the valley and the peak changed with Reynolds number. The difference of these two local heat fluxes decreased with increasing Reynolds numbers.

Comparison with other similar work has been made based on the present experimental correlation in a common range of Reynolds number. Heat transfer in this cross-corrugated channel was about 42% less than the one obtained by Sparrow and Comb [15]. The heat transfer was increased by 16 to 83 % by comparison with the result of Kirpikov et al. [17]. The heat transfer coefficient was about 2.8 times that of a smooth channel. Comparison of corresponding friction factors shows that the large heat transfer is at the expense of a large friction factor.

5.3 Mixed convection

The experimental results for mixed convection have been presented by comparison to 'pure' forced convection. It is noted that the present experimental results have shown phenomena quite similar to buoyancy-aided pipe flow [32]. In a range of small Grashof numbers, heat transfer was primarily by forced convection and heat transfer impairment due to flow laminarization for natural convection was not obvious in our results. This might be due to natural convection effects, which always appear in the forced convection correlation. In a range of large Grashof numbers, the heat transfer was observed to be larger than 'pure' forced convection but the increase was not significant. Natural convection did not appear to show significant influence over the forced convection in the extent of this experiments.

Chapter 6

RECOMMENDATIONS

6.1 Experimental apparatus

- As discussed in Chapter four, the actual thermal boundary condition in this study was neither uniform wall temperature nor uniform heat flux. When these two thermal boundary conditions are pursued, the thickness and material of the corrugated sheet and the way of heating have to be considered carefully beforehand.
- In a situation of very precise measurements, i.e. turbulence measurements, if electric heating has to be used, d.c. power supply to the heater is recommended to prevent the electrical noise. In the present experiment, the heated corrugated sheet picked up electrical noise from the a.c. electric radiant heaters. This noise overlapped with the expected sensor signal and transferred into the data acquisition through the sensors on the corrugated surface. The noise can be also filtered to some extent with certain filtering means but it is never easy to remove completely.
- The cross-corrugated channel is recommended for forced convection applications, since from this study it showed a good heat transfer performance with a reasonable pumping power (reasonable friction factor).

6.2 Future work

- Flow visualization should be conducted to understand the fluid flow behavior inside the channel which has great influence on the heat transfer. In order to do this, another apparatus should be designed with liquid as a working fluid, and transparent corrugated sheets have to be used.
- In order to minimize natural convection effects in forced convection correlation, the cross-corrugated channel should be placed horizontally with the heated corrugated sheet on the top of the channel. More attention should be paid to the forced convection study for its good heat transfer performance. Experiment should be conducted for more channel gaps.
- In order to predict the friction factor precisely, the pressure taps should be mounted on the corrugated surfaces. More taps should be used especially near the inlet of the channel to study the pressure drop along the flow direction. The friction factor study could be treated as a fluid mechanics problem so that no heating is required in this study, which will make it easier to place pressure taps on the corrugated surface.
- Results of the present study showed that the local heat transfer coefficient on the peak of the corrugation was larger than that on the valley, and Goldstein and Sparrow [11] found that the local heat transfer coefficient on the leeward facets was appreciably smaller than that on the windward facets in a corrugated channel. But it is still not clear how the local heat flux changes along the corrugation. It would be interesting to study how the local heat transfer changes along the corrugation and how this change depends on the Reynolds number.

- In the present experiment, the heating was asymmetric and the heated sheet corrugated along the main flow direction (z direction). It might also be interesting to investigate heat transfer situation when the heated sheet corrugates across the main flow direction. For present test section, the corrugated channel should be heated from the present insulated sheet and insulated from the present heated sheet.
- Numerical modelling of heat transfer in the cross-corrugated channel should be conducted.

Bibliography

- [1] Wirtz, R. A. and Stulzman, R. J., " Experiments on Free Convection Between Vertical Plates With Symmetric Heating, " *Journal of Heat Transfer*, Vol.104, 1982, pp.501-507.
- [2] Aung, W., Fletcher, L. S. and Sernas, V., " Developing Laminar Free Convection Between Vertical Plates and Asymmetric Heating, " *International Journal of Heat and Mass Transfer*, Vol.16, 1972, pp.2293-2308.
- [3] Eckert, D.R.G. and Jackson, T.W., " Analysis of Turbulent Free Convection Boundary Layer on Flat Plate, " NACA Report 1015, July 1950.
- [4] Sparrow, E. M. and Azevedo, L. F. A., " Vertical-Channel Natural Convection Spanning Between the Fully-Developed Limit and the Single-Plate Boundary-Layer Limit ", *International Journal of Heat and Mass Transfer*, Vol.28, 1985, pp.1847-1857.
- [5] Elenbaas, W., " Heat Dissipation of Parallel Plates by Free Convection, " *Physica*, Holland, Vol.9, No.1, 1942, pp.1 - 28.
- [6] Bodia, J. R. and Osterle, J. F., " The Development of Free Convection Between Heated Vertical Plates, " *Journal of Heat Transfer*, Vol. 84, 1962, pp.40-44.
- [7] Aung, W., " Fully Developed Laminar Free Convection Between Vertical Plates Heated Asymmetrically," *International Journal of Heat and Mass Transfer*, Vol.15, 1972, pp.1577-1580.
- [8] Sparrow, E. M., Chrysler, G. M. and Azevedo, L. F., " Observed Flow Reversals and Measured-Predicted Nusselt Numbers for Natural Convection in a One-Sided Heated Vertical Channel ", *Journal of Heat Transfer*, Vol.106, 1984, pp.325-332.
- [9] Churchill, S.W. and Usagi, R., "A General Expression for the Correlation of Rates of Transfer and Other Phenomena", *A.I.Ch.E. Journal*, Vol.18, 1972, pp.1121-1128.
- [10] Faghri, M. and Asako, Y., "Periodic, Fully Developed, Natural Convection in a Channel with Corrugated Confining Walls", *International Journal of Heat and Mass Transfer*, Vol.29, 1986, pp.1931-1936.
- [11] Goldstein, L. and Sparrow, E.M., "Experiments on the Transfer Characteristics of a Corrugated Fin and Tube Heat Exchanger Configuration", *Journal of Heat Transfer*, Vol.98, 1976, pp.26-34.

- [12] Goldstein, L. and Sparrow, E.M., "Heat/Mass Transfer Characteristics for Flow in a Corrugated Wall Channel", *Journal of Heat Transfer*, Vol.99, 1977, pp.187-195.
- [13] O'Brien, J.E. and Sparrow, E.M., "Corrugated-Duct Heat Transfer, Pressure Drop, and Flow Visualization", *Journal of Heat Transfer*, Vol.104, 1982, pp.410-416.
- [14] Sparrow, E.M. and Hossfeld, L.M., "Effect of Rounding of Protruding Edges on Heat Transfer and Pressure Drop in a Duct", *International Journal of Heat and Mass Transfer*, Vol.27, No.10, 1984, pp.1715-1723.
- [15] Sparrow, E.M. and Comb, J.W., "Effect of Interwall Spacing and Fluid Flow Inlet Conditions on a Corrugated-Wall Heat Exchanger", *International Journal of Heat and Mass Transfer*, Vol.26, No.7, 1983, pp.993-1005.
- [16] Molki, M., "Heat Transfer Characteristics of Corrugated Ducts with Variable Corrugation Angle", *Proceedings of the Eighth International Heat Transfer Conference*, San Francisco, USA, Vol.6, 1988, pp.2879-2884.
- [17] Kirpikov, V.A., Gutarev, V.V. and Tsirel'Man, N.M., "A Study of the Heat Transfer and Frictional Resistance in a Diverging-Converging Duct", *Heat Transfer-Soviet Research*, Vol.2, No.2, March 1970, pp.48-53.
- [18] Kirpikov, V.A. and Tsirel'Man, N.M., "Heat Transfer and Frictional Resistance in Turbulent Gas Flow in the Field of an Alternating Pressure Gradient", *Heat Transfer-Soviet Research*, Vol.3, No.2, March-April 1971, pp.116-121.
- [19] Amano, R.S., Bagherlee, A., Smith, R.J., and Niess, T.G. "Turbulent Heat Transfer in Corrugated-Wall Channels With and Without Fins", *Journal of Heat Transfer*, Vol.109, 1987, pp.62-67.
- [20] Asako, Y., and Nakamura H., "Heat Transfer and Pressure Drop Characteristics in a Corrugated Duct with Rounded Corners", *International Journal of Heat and Mass Transfer*, Vol.31, No.6, 1988, pp.1237-1245.
- [21] Metais, B., and Eckert, E.R.G., "Forced, Mixed and Free Convection Regimes", *Journal of Heat Transfer*, Vol.86, 1964, pp.295-296.
- [22] Quintiere, J. and Mueller, W.K., "An Analysis of Laminar Free and Forced Convection between Finite Vertical Parallel Plates", *Journal of Heat Transfer*, Vol.95, 1973, pp.53-59.
- [23] Dalbert, A.M., "Natural, Mixed and Forced Convection in a Vertical Channel with Asymmetric Uniform Heating", *Proceedings of the Seventh International Heat Transfer Conference*, Munich, F.R.G., Vol.1, 1982, pp.431-434.

- [24] Chato, J.C., "Combined Free and Forced Convection Flows in Channels", *Lectures on Advanced Heat Transfer*, ed. Chao, B.T., University of Illinois Press, 1969, pp. 439-459.
- [25] Hallman, T.M., "Experimental Study of Combined Forced and Free Laminar Convection in a vertical Tube", NASA Technical Note D-1104, 1961.
- [26] Baek, B.J., Palaski, D.A., Armaly, B.F. and Chen, T.S., "Mixed Convection in an Asymmetrically Heated Vertical Parallel-Plate Duct Flow", *Proceedings of the Ninth International Heat Transfer Conference*, Jerusalem, Israel, Vol.2, 1990, pp.369-374.
- [27] Habchi, S. and Acharya, S., "Laminar Mixed Convection in a Partially Blocked, Vertical Channel", *International Journal of Heat and Mass Transfer*, Vol.29, 1986, pp.1711-1722.
- [28] Kanevce, G. and Oka, O., "Correcting Hot-Wire Readings for Influence of Fluid Temperature Variations", *DISA Information*, No.15, November, 1973, pp.21-24.
- [29] *Analog Devices 1984 Databook*, Vol.1, Section 8, pp.31-38.
- [30] *Model 1010A Instruction Manual*, Thermo-Systems Inc., Minneapolis, Minnesota, USA
- [31] *Hot Wire/Hot film Anemometry Probes & Accessories*, Thermo-Systems Inc., Minneapolis, Minnesota, USA
- [32] *Dentec Probe Catalog*, Dentec Electronic Inc. Allendale, NJ, USA
- [33] Kreith, F. and Bohn, M.S., "Principles of Heat Transfer", Harper & Row, Publishers, New York, Fourth Edition, 1986.
- [34] Aung, W., "Mixed Convection in Internal Flow", *Handbook of Single-Phase Convective Heat Transfer*, ed. Kakac, S., John Willy & Sons, Inc., Chapter 15, 1987.
- [35] Holman, J.P., "Heat Transfer", McGraw-Hill Book Company, Sixth Edition, 1986, pp.333.
- [36] Jackson, J.D. and Hall, W.B., "Influences of Buoyancy on Heat Transfer to Fluids Flowing in Vertical Tubes under Turbulent Conditions", *Turbulent Forced Convection in Channels and Bundles*, ed. Kakac, S. and Spalding, D.B., Vol.2, pp.613-173, 1979.
- [37] Dittus, F.W. and Boelter, L.M.K., *Univ. Calif. Berkeley Publ. Eng.*, Vol.69, pp.433, 1930.

Appendix A

Sample Calculation

We choose a mixed convection case for gap 2 as a sample, and forced convection and natural convection are similar. Some known parameters for the sample case are listed below:

Length of the cross-corrugated channel L	=	667 (mm),
Width of the cross-corrugated channel W	=	437 (mm),
Hydraulic diameter of the channel D_h	=	57 (mm),
Gap of the extension channel b_e	=	44 (mm),
Mean spacing of the cross-corrugated channel b_m	=	31 (mm),
Ambient temperature T_∞	=	24.4 (°C).

The wall temperature readings at each position were obtained from the data acquisition and shown in Table A.9.(a). The fluid velocity and temperature profiles were measured as well and presented in Table A.9.(b). In the Table, T_w is the averaged local wall temperature and S_{T_w} is the standard deviation of the averaged local wall temperature, which are defined as:

$$T_w = \frac{\sum_{j=1}^N T_w(j)}{N}, \quad (\text{A.54})$$

and

$$S_{T_w} = \sqrt{\frac{\sum_{j=1}^N (T_w(j) - T_w)^2}{N}}, \quad (\text{A.55})$$

where N is the sampling number of data acquisition for each local wall temperature measurement and equals to 100 in the experiments.

Similarly, T_f and u are measured fluid temperature and velocity, S_{T_f} and S_u are their corresponding standard deviations. The definitions are shown in the following Appendix B: Error analysis.

No.(i)	T_w (°C)	S_{T_w} (°C)	No.(i)	T_f (°C)	S_{T_f} (°C)	u (m/s)	S_u (m/s)
1	47.9	1.4239	0	24.38	0.5723	0	0
2	55.9	1.4845	1	36.11	0.7197	0.64587	0.0975
3	59.8	1.7486	2	36.38	0.755	0.77379	0.0874
4	65.8	1.384	3	36.58	0.8181	0.80992	0.0772
5	70.8	1.412	4	36.69	0.765	0.83859	0.0779
6	76.3	1.3571	5	37.31	0.7474	0.83875	0.0828
7	80.8	1.8786	6	36.86	0.8348	0.85721	0.0851
8	84.6	1.5205	7	37.12	0.7447	0.84772	0.0766
9	85.3	1.4649	8	36.96	0.7426	0.86635	0.0872
10	83.2	1.8051	9	37.25	0.745	0.83828	0.0791
11	44.2	1.4747	10	36.95	0.7709	0.82833	0.096
12	55.9	2.0998	11	36.83	0.7412	0.79123	0.0817
13	66.4	1.9527	12	35.89	0.7512	0.76718	0.0914
14	77.6	1.4432	13	34.92	0.7409	0.70214	0.0797
15	84.7	6.3777	14	33.3	0.6836	0.5957	0.084
16	44.1	1.4737	15	32.25	0.7305	0.54056	0.0427
17	55.7	2.3008	16	31.92	0.8372	0.57709	0.0293
18	66.8	2.1506	17	24.4	0.57	0	0
19	76.7	1.4725					
20	81.5	1.3681					
21	87.3	1.445					
22	86.9	1.4464					
23	76.2	2.278					
24	73.6	2.7477					

(a). T_w readings

(b). T_f and u readings

Table A.9: The original data from data acquisition.

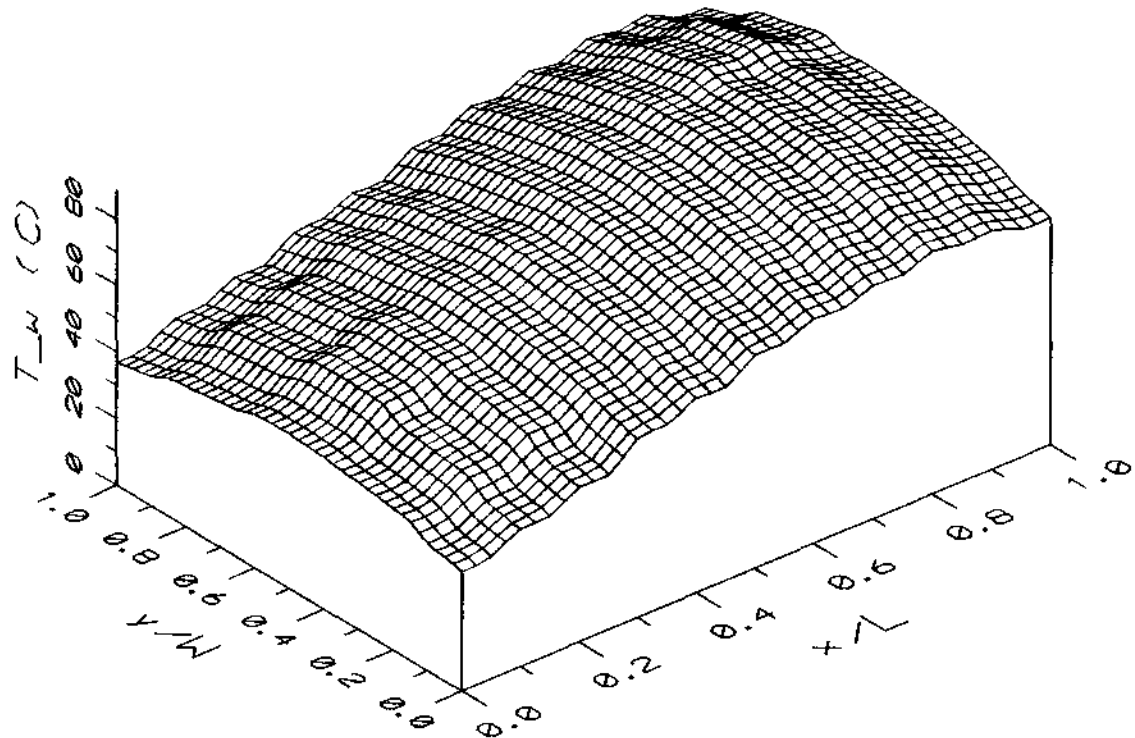


Figure A.20: Wall temperature distribution on the heated sheet.

A.1 Wall temperature

The wall temperature of the heated corrugated sheet was measured at twenty four points on the sheet. At each point, the sampling frequency and sampling time of the data acquisition are 20 Hz and 5 seconds.

For visual convenience, the wall temperature distribution on the heated corrugated sheet was plotted by both interpolating and extrapolating the data in Table A.9.(a) and is shown in Fig.A.20.

From the above figure, the wall temperature periodically changes along the flow direction due to the corrugations and the temperature at the peak is about 5 percent lower than that at the valley. This is because the local heat transfer coefficient at the valley is lower than that at the peak which leads to an increase of local wall temperature and a decrease of local heat flux across the wall at the valley.

From Fig.A.20, the wall temperature variation across the flow direction, was higher at the center and lower at the two ends. This was due to the way of heating. The radiant heaters were supposed to generate a uniform heat flux at their radiant surfaces. Since the surfaces were about 2 inches apart from the heated sheet, the shape factor from center point of the heated sheet to the surfaces was higher than that from point at the edge of the sheet to the surfaces. This would result in a highest local heat radiance at the center of the sheet and lowering heat radiance away from the center. The average wall temperature across the flow direction at a fixed x value was about five percent lower than the temperature at the center.

An averaged wall temperature has been used in our heat transfer correlation. This wall temperature is obtained by averaging the wall temperatures at each peak of the corrugation which is

$$\bar{T}_w = \frac{1}{10} \sum_{i=1}^{10} T_w(i) = 71.0 \text{ } (^{\circ}C). \quad (A.56)$$

From the above analysis and the way the averaged wall temperature was calculated, the T_w was close to the temperature obtained by averaging the overall heat corrugated sheet temperatures.

A.2 Mean velocities and bulk temperatures of the fluid

The temperature and velocity profiles of the fluid were measured across the gap of the extension channel at its exit. The sampling rate was 10 Hz and the sampling time was 20 seconds for each sampling. The fluid temperature was used to compensate the velocity deviation due to temperature difference from the calibration temperature. It was also used to obtain the fluid bulk temperature at the outlet of the corrugated channel. The profiles are obtained through travelling the thermocouple and hot-wire probes across the extension channel at the measuring section. The velocity in the figure has already been compensated for the fluid temperature difference from the calibration temperature which is directly done by the data acquisition program. Air velocity at the extension channel wall was set to be zero by considering the fluid viscosity. Air temperature at the wall was set to be equal to the ambient temperature which was validated in appendix D. Figure A.21 shows the air velocity and temperature profiles at the measurement section.

The mean velocity at the measurement section is obtained through numerically integrating Eq.(4.18), which turns out to be for this case:

$$U = \frac{1}{b_e} \left[\left(\sum_{i=1}^{16} u(i) \frac{b_e}{17} \right) + \frac{1}{4} \left(\frac{u(1) + u(16)}{2} \right) \frac{b_e}{17} \right] = 0.775 \text{ (m/s)}. \quad (\text{A.57})$$

The inlet bulk temperature of the fluid was set to be equal to the ambient temperature T_∞ which was measured at the inlet of the corrugated channel. The sampling rate was 10 Hz and sampling time was 20 seconds.

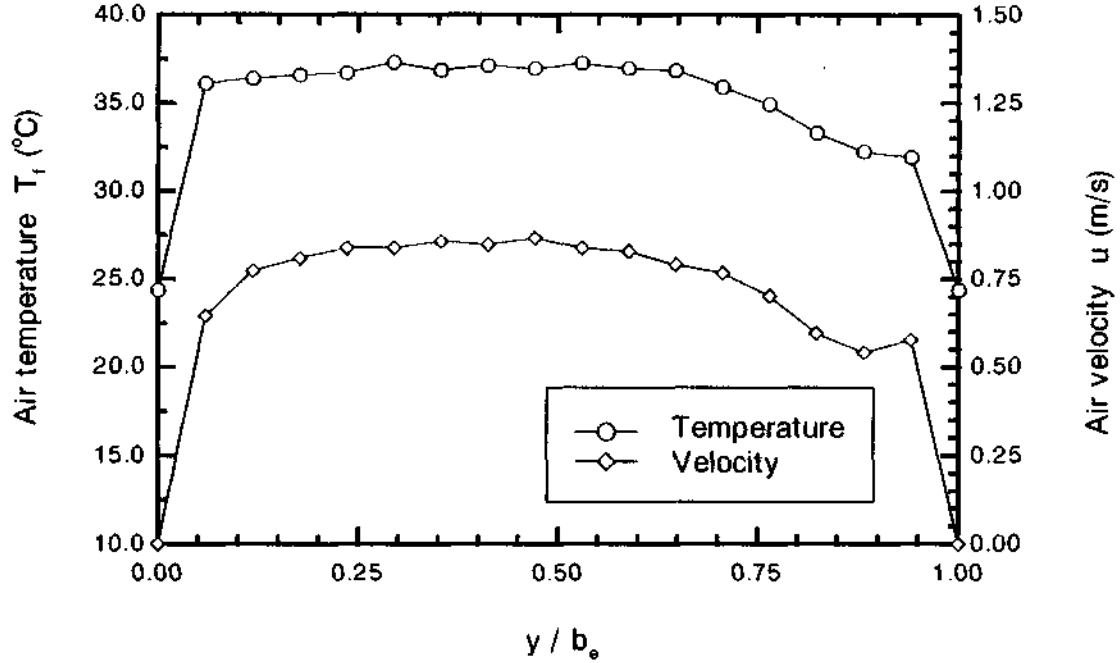


Figure A.21: Air velocity and temperature profiles.

The outlet bulk temperature of the fluid T_{bo} is obtained through numerically integrating Eq.(4.21),

$$T_{bo} = \frac{1}{b_e} \left[\left(\sum_{i=1}^{16} u(i)T_f(i) \frac{b_e}{17} \right) + \frac{1}{4} \left(\frac{u(1)T_f(1) + u(16)T_f(16)}{2} \right) \frac{b_e}{17} \right] = 35.8 \text{ (}^\circ\text{C)}. \quad (\text{A.58})$$

The mean bulk air temperature is defined as the average temperature of the inlet and outlet bulk air temperatures,

$$\bar{T}_b = \frac{1}{2}(T_\infty + T_{bo}) = 30.1 \text{ (}^\circ\text{C)}.$$

The mean velocity at the inlet of the corrugated channel U_0 is obtained by applying the

mass conservation in the channels,

$$U_0 = \frac{\rho U W b_e}{\rho_0 U_0 W b_m} = 1.059 \text{ (m/s)},$$

where ρ_0 and ρ are evaluated at T_∞ and T_{bo} respectively, and $\rho_0 = 1.1463 \text{ kg/m}^3$ and $\rho = 1.1038 \text{ kg/m}^3$.

Heat Transfer rate from the heated sheet to the fluid is derived from calculation, since the corrugated channel and the extension channel are thermally insulated. From energy balance, the heat input from the heated sheet is equal to the enthalpy flux across the channels,

$$Q = \rho U W b_e c_p (T_{bo} - T_\infty) = 195 \text{ (W)},$$

where ρ and c_p are evaluated at T_{bo} and $\rho = 1.1038 \text{ kg/m}^3$, $c_p = 1013.8 \text{ J/kg K}$.

A.3 Sample calculation

In the experiment of mixed convection, the wall temperature and fluid bulk temperature difference is quite high and the film temperature has been used for the evaluation of the fluid properties.

$$T_{film} = \frac{\bar{T}_b + T_w}{2} = 50.6 \text{ (}^\circ\text{C)}.$$

The properties were originally taken from Kreith and Bohn's book [31], and they were interpolated with linear regression for a specific temperature. Prandtl number for air is constant and equal to 0.71 in the range of temperatures of the experiments. At the film temperature of 50.6 °C, the fluid properties are listed below:

$$\begin{aligned}
\rho &= 1.10535 \text{ (kg/m}^3\text{)}, \\
\beta &= 3.1 \times 10^{-3} \text{ (1/K)}, \\
c_p &= 1015.6 \text{ (J/kg K)}, \\
k &= 0.02725 \text{ (W/m K)}, \\
\mu &= 1.955 \times 10^{-5} \text{ (N s/m}^2\text{)}, \\
\nu &= 1.862 \times 10^{-5} \text{ (m}^2\text{/s)}.
\end{aligned}$$

From the above properties and given parameters, the following heat transfer dimensionless terms can be calculated:

$$Re_D = \frac{\rho U_0 D_h}{\mu} = 3400,$$

$$Gr_D = \frac{\beta g (T_w - \bar{T}_b) D_h^3}{LW k \nu^2} = 6.575 \times 10^5,$$

$$Ra_D = Gr_D Pr = 4.668 \times 10^5,$$

$$Nu_D = \frac{Q D_h}{LW k (T_w - \bar{T}_b)} = 34.1,$$

$$Gr_L = \frac{\beta g (T_w - \bar{T}_b) L^3}{LW k \nu^2} = 5.288 \times 10^6,$$

$$Ra_L = Gr_L Pr = 3.754 \times 10^5,$$

$$Nu_L = \frac{QL}{LW k (T_w - \bar{T}_b)} = 399.0.$$

Appendix B

Error analysis

B.1 Wall temperature measurement

The error of the wall temperature measurement is associated to the process of data acquisition. The voltage through the J-type thermocouples is first input to AD594C which is a monolithic thermocouple amplifier with cold temperature compensation. The calibration accuracy is of $\pm 1^\circ\text{C}$.

The local wall temperature T_w was an averaged value of the N samples from the data acquisition,

$$T_w = \frac{\sum_{j=1}^N T_w(j)}{N}.$$

The error in the local wall temperature associated with the temperature signal is the standard error of the signal. The standard deviation of the local mean wall temperature is

$$S_{T_w} = \sqrt{\frac{\sum_{j=1}^N (T_w(j) - T_w)^2}{N}},$$

where N is the number of samples for each local wall temperature measurement and equals to 100. Since S_{T_w} is less than 3°C in most cases, the standard error:

$$\varepsilon_{T_w} = \frac{S_{T_w}}{\sqrt{N}} = \frac{S_{T_w}}{10}. \quad (\text{B.59})$$

Therefore the error caused by the uncertainty of the signal is about 0.3°C . The error of the combined effects in the local wall temperature is about $\pm 1.3^\circ\text{C}$.

B.2 Air velocity measurement

The error in air velocity measurement is associated with the hot-wire anemometry. In our experiment, the output of the bridge voltage and fluid velocity are related through the following equation at the calibration condition:

$$E^2 = B_1 + B_2 (u)^n$$

During calibration, the velocity was calibrated against a Pitot tube manometer. The velocity from the manometer was related by,

$$\frac{1}{2}\rho u^2 = \rho_{Al} g h, \quad (\text{B.60})$$

where ρ_{Al} was the density of alcohol and h was the vertical height of the alcohol column in the Pitot tube manometer. A scale of 1:25 declination of the column was chosen in the calibrations. The reading from the column gave an accuracy of ± 0.25 mm. Converting this accuracy to the vertical height scale gives the error from reading $\Delta h = \pm 0.01$ mm. From differentiating the above equation, the error in air velocity from reading the column scale is,

$$\begin{aligned} \varepsilon_u &= \left(\frac{\partial u}{\partial h} \right) \Delta h \\ &= \sqrt{\frac{\rho_{Al} g h}{2\rho}} \frac{1}{\sqrt{h}} \Delta h \\ &= \left(\frac{\rho_{Al} g}{\rho u} \right) \Delta h. \end{aligned} \quad (\text{B.61})$$

At a room temperature, say 20 °C, $\rho = 1.164$ kg/m³ and $\rho_{Al} = 806.6$ kg/m³, the above equation can be simplified to

$$\varepsilon_u = \frac{0.068}{u}. \quad (\text{B.62})$$

The error is inversely proportional to air velocity. The velocity is calibrated at a range of 0.4 ~ 6.5 m/s, and the error with respect to these two limits is in a range of 0.17 m/s to 0.01 m/s. The calibration curves also show more scattered points in the low velocity range. The above analysis doesn't account the effect of speed fluctuation and shift of the fan of the wind tunnel.

It should be noted that in our application, we use the developed fitting functions of calibration in predicting air velocity instead of using calibration points. The error of bridge voltage E is related to the fan speed shift and ambient temperature shift and we assume these errors are negligible during calibration. The standard deviation of air velocity regression S_u can be expressed as:

$$S_u^2 = \sqrt{\frac{\sum_{i=1}^N (u - u_{reg})^2}{N}}, \quad (\text{B.63})$$

where N is the number of calibration points and u_{reg} is the velocity from the regression. The standard deviations for probe1 and probe2 are 0.034 m/s and 0.029 m/s respectively.

Besides the calibration error, we have to consider the practical situation in which the fluid temperature is different from the calibration temperature. We used temperature correction to compensate this effect,

$$E_c = E \left(\frac{T_{wire} - T_{cal}}{T_{wire} - T_f} \right)^{0.5}.$$

This correction suggested by Kanevce and Oka [28] compensates the fluid temperature variation very well over large velocity range (i.e. velocity is larger than 2.5 m/s). The lower the velocity, the larger the error when using the above correction. At a velocity

of 0.14 m/s and a temperature range of $\pm 15^\circ\text{C}$ around the calibration temperature, the relative error in velocity is $\pm 4\%$.

The low velocity and high temperature flow situation took place in our natural convection experiment. The maximum fluid temperature above the calibration temperature was 14°C and the velocity in this case was 0.5 m/s. The minimum fluid velocity was 0.15 m/s and the corresponding fluid temperature was 3°C above the calibration temperature. We can see that the relative error in velocity at our extreme cases is less than $\pm 4\%$ and 3% might be a good estimate for these extreme cases.

From the above analysis, we can see that the maximum error appeared in the smallest velocity and it can be as much as 20% high. This is because at small velocity range, velocity was predicted with the calibration regression function and it is out of the calibration range. We predict the error in this small velocity range with the standard deviation of calibration regression. At higher velocity range, say higher than 2 m/s, the relative error in velocity is less than 3%.

B.3 Bulk air temperature measurement

The inlet bulk air temperature is the ambient temperature and it is measured with the same AD594C thermocouple amplifier which gives a calibration accuracy of $\pm 1^\circ\text{C}$. Considering the uncertainty of the temperature signal, the error is the standard error of the sampling signal and less than 0.1°C . Therefore the error in the inlet bulk air temperature caused by the combined effects is $\pm 1.1^\circ\text{C}$.

The outlet bulk temperature T_{bo} is calculated through measuring temperature and velocity profiles. The calculation of T_{bo} is simplified as following for the convenience of error analysis:

$$T_{bo} \approx \frac{\Delta b_e}{U b_e} \left(\sum_{i=1}^N u(i) T(i) \right), \quad (\text{B.64})$$

where Δb_e is the step distance of the profile measurement and $b_e = N \Delta b_e$. The error $\varepsilon_{T_{bo}}$ of the outlet bulk temperature T_{bo} is related by,

$$\varepsilon_{T_{bo}}^2 = \left(\frac{\Delta b_e}{U b_e} \right)^2 \left(\sum_{i=1}^N u(i)^2 \varepsilon_{T(i)}^2 + \sum_{i=1}^N T(i)^2 \varepsilon_{u(i)}^2 \right), \quad (\text{B.65})$$

where N is the number of samples for each velocity and temperature measurement. $\varepsilon_{T(i)}$ and $\varepsilon_{u(i)}$ are errors in the fluid temperature and velocity measurements respectively. Since the 20% relative error in velocity is brought by the method of velocity measurement, in the above equation, the error in velocity considered here should be the error caused by uncertainty of the velocity signal, which is the standard error of the velocity signal:

$$\varepsilon_{u(i)} = \frac{S_u}{\sqrt{N}} = \frac{S_u}{\sqrt{200}}, \quad (\text{B.66})$$

where N is the samples for each velocity measurement and equal to 200 in our experiment. This makes the relative error in $u(i)$ signal about 1%.

Similarly, the error in the fluid temperature caused by uncertainty of the temperature signal is less than 0.1°C which leads to the relative error in the fluid temperature to be less than 0.5%. The error in the bulk temperature caused by the uncertainty of the velocity and temperature measurement is less than 0.15°C. Therefore the uncertainty of the outlet bulk temperature is less than $\pm 1.2^\circ\text{C}$.

B.4 Heat transfer rate

The heat transfer rate Q equals to the enthalpy flux across the channel. The error of its measurement is associated with the error of the fluid bulk temperature difference across the channel. The error ε_Q of the heat transfer rate is related by

$$\varepsilon_Q^2 = \left(\frac{\partial Q}{\partial \Delta T} \right)^2 \varepsilon_{\Delta T}^2 + \left(\frac{\partial Q}{\partial U} \right)^2 \varepsilon_U^2, \quad (\text{B.67})$$

where

$$\Delta T = T_{b_o} - T_{\infty}.$$

Since the temperatures T_{b_o} and T_{∞} were measured with the same amplifier and same type of thermocouple wire, the error $\varepsilon_{\Delta T}$ of the bulk temperature difference was related by,

$$\varepsilon_{\Delta T}^2 = \varepsilon_{T_{b_o}}^2 + \varepsilon_{T_{\infty}}^2. \quad (\text{B.68})$$

Here the errors considered are the uncertainties of temperature signals. With the above analyzed 0.3% relative error in air temperature, $\varepsilon_{T_{b_o}}$ and ε_{∞} are 0.11°C and 0.06°C, when T_{b_o} and T_{∞} are 35°C and 20°C respectively. In this case, $\varepsilon_{\Delta T}$ takes a value of 0.13°C. The minimum value of ΔT was 2.3°C in our experiment and the relative error in ΔT was 5.7%. Therefore the error caused by the uncertainty of ΔT is very small compared to the 20% error of the velocity measurement. The uncertainty of heat flow rate ε_Q was about 20%.

B.5 Dimensionless terms

The uncertainty of Re_D is directly associated to the accuracy of velocity measurement and can be expressed as:

$$\varepsilon_{Re} = \left(\frac{\partial Re_D}{\partial U_0} \right) \Delta U_0. \quad (\text{B.69})$$

We may also write,

$$\frac{\varepsilon_{Re}}{Re_D} = \frac{\varepsilon_{U_0}}{U_0} \approx \frac{\varepsilon_U}{U}. \quad (\text{B.70})$$

The minimum velocity appeared in forced and mixed convection experiment is 0.72 m/s. Since the standard deviation of the velocity calibration regression is 0.034 m/s, the relative error in velocity is about 5%. The relative error in velocity caused by the temperature compensation is about 3%. The error caused by the combined effects is about 8%. Therefore the uncertainty in Re_D number is about 8%.

The error of Gr_D is directly associated to the accuracy of T_w and \bar{T}_b measurement and can be expressed as:

$$\varepsilon_{Gr} = \left(\frac{\partial Gr_D}{\partial \Delta T_{w\infty}} \right) \Delta T_{w\infty} = Gr_D \left(\frac{\varepsilon_{\Delta T_{w\infty}}}{\Delta T_{w\infty}} \right), \quad (\text{B.71})$$

where

$$\Delta T_{w\infty} = \bar{T}_w - T_\infty$$

for natural convection. For mixed convection, ΔT_{wb} is used in place of $\Delta T_{w\infty}$,

$$\Delta T_{wb} = \bar{T}_w - \bar{T}_b.$$

Since the wall temperature and the bulk temperature were both measured with the same thermocouple amplifier, the error considered here was only associated with the uncertainty of the temperature signals. For natural convection, we have

$$\varepsilon_{\Delta T_{wb}}^2 = \varepsilon_{T_w}^2 + \varepsilon_{T_\infty}^2. \quad (\text{B.72})$$

For mixed convection, we have

$$\varepsilon_{\Delta T_{wb}}^2 = \varepsilon_{T_w}^2 + \varepsilon_{\bar{T}_b}^2. \quad (\text{B.73})$$

Taking values of 0.3°C and 0.1°C for ε_{T_w} and $\varepsilon_{\bar{T}_b}$ respectively, the uncertainty in the temperature difference $\varepsilon_{\Delta T_{wb}}$ and $\varepsilon_{\Delta T_{w\infty}}$ is about 0.3°C . The minimum temperature difference ΔT_{wb} and $\Delta T_{w\infty}$ is about 7.0°C . Therefore the relative error in Grashof number is less than 5%

Since different definitions were used for Nusselt number in natural convection, forced and mixed convection, it is necessary to analyze the errors separately. In natural convection, the error in Nusselt number was associated with the accuracy of heat transfer rate Q measurement and the temperature difference measurement between the wall and the fluid ambient. The error can be written as:

$$\left(\frac{\varepsilon_{Nu}}{Nu}\right)^2 = \left(\frac{\varepsilon_Q}{Q}\right)^2 + \left(\frac{\varepsilon_{\Delta T_{w\infty}}}{\Delta T_{w\infty}}\right)^2. \quad (\text{B.74})$$

The minimum temperature difference $\Delta T_{w\infty}$ is about 12°C in natural convection. The relative error in the temperature difference is 2.5%. Therefore the relative error in Nusselt number Nu is about 20% for natural convection.

Under the forced and mixed convection, the error in Nusselt number was associated with the accuracy of heat transfer rate Q measurement and the temperature difference measurement between the wall and the fluid bulk mean. The error is related by,

$$\left(\frac{\varepsilon_{Nu}}{Nu}\right)^2 = \left(\frac{\varepsilon_Q}{Q}\right)^2 + \left(\frac{\varepsilon_{\Delta T_{wb}}}{\Delta T_{wb}}\right)^2. \quad (\text{B.75})$$

The minimum temperature difference ΔT_{wb} is about 2.3°C in natural convection. The relative error in the temperature difference is 13%.

The minimum velocity appeared in the forced and mixed convection experiment is 0.72 m/s . Since the standard deviation of the velocity calibration regression is 0.034

m/s, the relative error in velocity is about 5%. The relative error in velocity caused by the temperature compensation is about 3%. The relative error in velocity caused by the combined effects is about 8%. As the error analysis for the heat transfer rate, the relative error in the bulk temperature difference ΔT is 5.7% for forced and mixed convections. This makes the relative error in the heat transfer rate about 10%. Therefore the relative error in Nusselt number Nu_D is less than 17%. The summarized error analysis is listed in Table B.10.

Wall temperature T_w	1.3°C
Inlet bulk air temperature T_∞	1.1°C
Outlet bulk air temperature T_{bo}	1.2°C
Air velocity U	20%
Heat transfer rate Q	20%
Reynolds number Re_D	8%
Grashof number Gr_D, Gr_L	5%
Nusselt number Nu_D, Nu_L	20% (natural convection)
"	17% (forced and mixed)

Table B.10: Summary of error analysis.

Appendix C

Estimation of Radiation Heat Transfer

Under the natural and the mixed convective heat transfer, surface temperature of the heated sheet was usually high compared to the fluid temperature. The radiation heat transfer has to be estimated for this situation. The estimation is performed for natural convection case at which the surface temperature is maximum. The mean beam length method is used to evaluate the radiation effect. The corrugated sheets are assumed to be grey body, and the hemispherical emittance $\epsilon_w \approx 0.50$. The known parameters for the chosen gap2 case are listed below:

$$T_\infty = 27.8 \text{ (}^\circ\text{C)} = 301 \text{ (K)},$$

$$T_{bo} = 51.7 \text{ (}^\circ\text{C)} = 325 \text{ (K)},$$

$$\bar{T}_w = 115^\circ\text{C} = 388 \text{ (K)},$$

$$Q = 318 \text{ (W)},$$

$$\phi = 42 \% \text{ (from } T_{dry} = 27^\circ\text{C}, T_{wet} = 18^\circ\text{C)}.$$

Relative humidity of atmosphere was obtained from the Psychrometric Chart. The dry bubble and wet bubble temperatures of atmosphere were taken every experiment day. In most of the experimental conditions, relative humidity of the atmosphere was in a range of 40 ~ 60 %. Here $\phi = 80\%$ is used in the estimation. The saturation pressure of the water vapor at 27.8°C is

$$p_s = 0.03768 \text{ (bar)}.$$

The partial pressure of the water vapor p_{wv} is

$$p_{wv} = \phi p_s = 0.03014 \text{ (bar)}. \quad (\text{C.76})$$

Due to the rough geometry of the cross-corrugated channel, an effective mean beam length L_{mb} of the channel has to be used,

$$L_{mb} = \frac{3.4 V_{flow}}{A_{wetted}} = 0.85 D_h = 0.048 \text{ (m)}. \quad (\text{C.77})$$

Therefore,

$$p_{wv} L_{mb} = 0.00145 \text{ (bar m)} = 0.0015 \text{ (atm m)}.$$

From Figure 9.45 of Kreith and Bohn's book [33], at mean bulk temperature of the fluid \bar{T}_b of 40°C, the emittance ϵ_{wv} of water vapor is about 0.018. The absorptance of the water vapor α_{wv} is

$$\alpha_{wv} = C_{wv} \epsilon'_{wv} \left(\frac{T_{wv}}{T_w} \right)^{0.45}, \quad (\text{C.78})$$

where T_{wv} = water vapor temperature (°C),

ϵ'_{wv} = water vapor emittance evaluated at T_w and $p_{wv} L_{mb} (\bar{T}_w / T_{wv})$,

C_{wv} = 1 at pressure of 1 atm.

The calculation results are:

$$\epsilon'_{wv} = 0.017,$$

$$\alpha_{wv} = 0.0153.$$

The heat transfer rate by radiation from the heated corrugated sheet to the water vapor is equal to the difference of the absorbed and emitted radiation by the water vapor,

$$q_r = \sigma A_{wetted} (\alpha_{wv} \epsilon_w \bar{T}_w^4 - \epsilon_{wv} T_{wv}^4) = 0.024 \text{ (W)}, \quad (\text{C.79})$$

where σ is Stefan-Boltzmann constant and equals to 5.67×10^{-8} (W/m² K⁴), A_{wetted} is the wetted area of the corrugated channel and equals to 0.692 (m²).

From calculation, the radiation heat transfer is only about 0.01% of the total heat transfer. The radiation effect in this experiment is negligible.

Appendix D

Estimation of Heat Loss through the Insulated Walls

In the analysis of heat transfer process, An assumption was made that there was no heat loss through the walls of the extension section and test section. In practice, there is always heat transfer when temperature gradient exists. The heat loss is estimated in the following sections. In this experiment, the heat loss consists of the loss through the extension channel and the loss through the cross-corrugated channel.

D.1 Heat loss through the extension channel

The heat loss through the wall of the extension channel is illustrated in Fig. D.22. The process of heat loss goes through the following procedure. The fluid has been heated up before entering the extension channel. The heated fluid transfers the heat by a rate of q_f to the inner wall of plywood board by forced convective way. The heat then transfers through the plywood board and ceramic blanket by conductive way, and dissipates to the environment by natural convective way.

In the estimation, it is assumed that the outer surface temperature of the ceramic blanket equals to the ambient temperature T_∞ . This assumption will lead to an over-estimate of the heat loss, since the heat resistance through natural convection from the ceramic blanket to the environment is neglected.

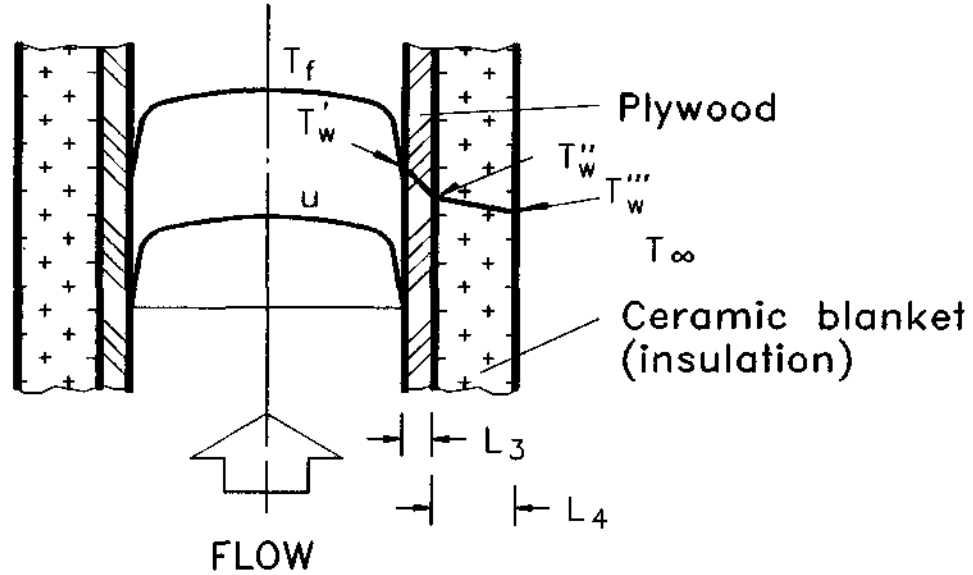


Figure D.22: Heat loss through the extension channel.

The heat loss rate q_l is coupled through the following equations:

$$\frac{q_l D'_h}{(T_b - T'_w) k} = C(Re'_D)^n, \quad (\text{D.80})$$

$$q_l = \frac{k_l}{L_3 + L_4} (T'_w - T_\infty), \quad (\text{D.81})$$

where Re'_D is Reynolds number based on the hydraulic diameter D'_h of the extension channel, T'_w is the inner wall temperature of the plywood, C and n are constants, and k_l is the combined heat conductivity of the plywood and the ceramic blanket,

$$k_l = (L_3 + L_4) / \left(\frac{L_3}{k_3} + \frac{L_4}{k_4} \right), \quad (\text{D.82})$$

where k_3 and k_4 are the heat conductivities of the plywood and the ceramic blanket respectively. The heat loss q_l can be expressed as:

$$q_l = h_l (T_b - T_\infty), \quad (\text{D.83})$$

where h_l is the heat loss coefficient for the extension channel. From the above equations, h_l can be expressed as:

$$h_l = \left(\frac{L_3 + L_4}{k_t} + \frac{D'_h}{k C (Re'_D)^n} \right)^{-1}. \quad (\text{D.84})$$

The fixed parameters in the above analysis are listed below:

$$\begin{aligned} D'_h &= 0.121 \text{ (m) for gap1, and } 0.080 \text{ (m) for gap2,} \\ L_3 &= 0.013 \text{ (m),} \\ k_3 &= 0.109 \text{ (W/m K),} \\ L_4 &= 0.025 \text{ (m),} \\ k_4 &= 0.035 \text{ (W/m K),} \\ k &= 0.0251 \text{ (W/m K) at } 20^\circ\text{C.} \end{aligned}$$

Since the combined heat loss conductivity k_t is a constant when the insulation materials are chosen, the heat loss coefficient h_l reaches its maximum when Reynolds number Re'_D is maximum. The heat loss rate q_l reaches its maximum with the maximum bulk temperature difference between the inlet and the outlet of the test section at the maximum h_l .

Considering these factors, a case of mixed convection is chosen for the estimation, in which the flow reached its maximum bulk temperature increase with the largest Reynolds number. The known parameters are listed below:

$$\begin{aligned}
D'_h &= 0.121 \text{ (m)} \\
T_\infty &= 22.0 \text{ (}^\circ\text{C)} \\
T_{bo} &= 31.2 \text{ (}^\circ\text{C)} \\
Re'_D &= 38400 \\
Q &= 1690 \text{ (W)}
\end{aligned}$$

Using Dittus-Boelter [37] correlation for cooling,

$$Nu_D = 0.023 Re_D^{0.8} Pr^{0.3}, \quad (\text{D.85})$$

the constants C and n in Eq.(D.80) can be determined:

$$\begin{aligned}
C &= 0.023 Pr^{0.3} = 0.021, \\
n &= 0.8.
\end{aligned}$$

With these known parameters, others can be calculated:

$$\begin{aligned}
h_t &= 1.12 \text{ (W/m}^2 \text{ K)}, \\
q_t &= 10.3 \text{ (W/m}^2\text{)}.
\end{aligned}$$

The heat loss through the extension channel Q'_t is:

$$Q'_t = q_t A_e = 4.2 \text{ (W)}, \quad (\text{D.86})$$

where A_e is the wetted area of the extension channel. From Eq.(D.81), T'_w can be solved and equals to 22.1°C.

D.2 Heat loss through the cross-corrugated channel

The heat loss through the cross-corrugated channel consists of heat loss through the insulated corrugated sheet and the two side walls in the test section. This corrugated

sheet is straight along the flow direction. It is treated here as flat channel convective heat transfer. The bulk temperature increased from the ambient temperature T_∞ to the outlet bulk temperature T_{b_o} . Therefore the mean bulk temperature \bar{T}_b is used in the calculation of heat loss. If the heat loss coefficient for the extension channel is used here, the heat loss through the corrugated channel Q_i'' is:

$$Q_i'' = h_t (\bar{T}_b - T_\infty) A_t = 1.9 \text{ (W)}. \quad (\text{D.87})$$

where A_t is the wetted area of the insulated corrugated sheet and the side walls. The total heat loss Q_i is the sum of the heat losses through the corrugated channel and the extension channel:

$$Q_i = Q_i' + Q_i'' = 5.1 \text{ (W)}. \quad (\text{D.88})$$

The total heat transfer rate Q in this considered case is 1690 W. Therefore there is about 0.3% relative heat loss.

The above estimated Q_i was the maximum heat loss in this experiment. The minimum heat transfer rate Q in the forced and the mixed convection experiment was 62.5 W. In this case, we have

$$\begin{aligned} Re'_D &= 11600, \\ T_\infty &= 23.1 \text{ }^\circ\text{C}, \\ T_{b_o} &= 24.2 \text{ }^\circ\text{C}. \end{aligned}$$

With the same procedure, the heat loss can be calculated:

$$\begin{aligned} h_t &= 1.03 \text{ (W/m}^2 \text{ K)}, \\ Q_i &= 0.87 \text{ (W)}. \end{aligned}$$

Therefore there was about 1.4% heat loss in this situation. The above analysis shows that the heat loss from the insulation is negligible for forced and mixed convection experiment.

From the above estimations, the effect of the forced convective part on the heat loss coefficient was very small due to the effective insulation. The maximum relative heat loss occurred when the fluid temperature gradient was maximum and the heat transfer rate was minimum. This occurred in natural convection situation.

In natural convection, $Nu = C(Ra)^m$, which can be interpreted as:

$$\frac{Q}{T_w - T_\infty} \propto (T_w - T_\infty)^m.$$

The heat transfer loss Q_l is proportional to the temperature difference of the outlet and the inlet of the channel,

$$Q_l \propto (T_{bo} - T_\infty) \propto (T_w - T_\infty).$$

Therefore we have,

$$\frac{Q_l}{Q} \propto \frac{1}{(T_w - T_\infty)^m},$$

where m is about 0.9 in this experiment. This means that the relative heat loss reaches its maximum when the temperature difference is minimum. This is the case when the heat transfer rate is minimum in the natural convection. The known parameters for the chosen case for gap1 are listed below:

$$\begin{aligned} Re_D &= 640, \\ T_\infty &= 21.5 \text{ (}^\circ\text{C)}, \\ T_{bo} &= 23.5 \text{ (}^\circ\text{C)}, \\ Q &= 5.8 \text{ (W)}. \end{aligned}$$

The fluid was laminar under this condition and the Nusselt number was about 5.1 [33]. This means in Eq.(D.80), $C(Re'_D)^n$ should be replaced with 5.1. With these known parameters, the others can be obtained,

$$h_l = 0.72 \text{ (W/m}^2 \text{ K)},$$

$$q_l = 1.44 \text{ (W/m}^2 \text{)},$$

$$Q_l = 0.4 \text{ (W)}.$$

Therefore the relative heat loss in this situation was 6.9 %. In most cases, the relative heat loss was small and the assumption of neglecting heat loss through the insulation was valid except that in a few natural convection cases with very low heat transfer rate, the relative heat loss was a little high.